



Norwegian University of
Science and Technology

Minimum Ignition Energy in a Hydrogen Combustible Mixture

Jens Tarjei Jensen

Master of Science in Physics and Mathematics

Submission date: June 2011

Supervisor: Ingve Simonsen, IFY

Co-supervisor: Nil Erland Haugen, SINTEF
Morten Seljeskog, SINTEF

Faculty of Natural Sciences and Technology
Department of Physics



MASTER'S THESIS

Minimum Ignition Energy in a Hydrogen
Combustible Mixture

Jens Tarjei JENSEN

Supervisors: Nils Erland L. HAUGEN & Morten SELJESKOG

June 28, 2011

Abstract

In this thesis the Minimum Ignition Energy, in a hydrogen-air system, is studied by Direct Numerical Simulations (DNS) in a program called the Pencil Code. The heat source used to achieve ignition is modeled by a Gaussian temperature distribution. Three different geometries of the heat source are looked upon, one with spherical geometry in three dimensions, one with cylindrical geometry in two dimensions and the last in one dimension. The results show that the dimensionality of the heat source has a strong impact on ignition.

In addition, a new simpler zero dimensional simulation method is proposed with the goal of replicating the results from the Pencil Code. This method needs less calculation power, and uses ignition delay time data together with the heat equation to simulate ignition. The model has proven itself useful since it reproduces the Pencil Code results very well.

Preface

This master thesis is the final part of my degree in Master of Science and Technology (Sivilingeniør) at the Norwegian University of Science and Technology in Trondheim, NTNU. It is done in collaboration with SINTEF Energy Research. The thesis covers 30 credit units.

Acknowledgements

I would like to thank my supervisors Nils Erland L. Haugen and Morten Seljeskog at SINTEF Energy Research for their guidance and invaluable help during this thesis. I will also give my thanks to Prof. Ingve Simonsen at the Department of Physics for being my formal supervisor. In addition I would like to say thank you to all my fellow students which shared the same studying hall.

Contents

Preface	III
List of Figures	VII
List of Tables	VIII
1 Introduction	1
2 Theory	3
2.1 Chain reactions	3
2.2 Explosion limits and the oxidative characteristics of hydrogen	4
2.3 Stoichiometry and the equivalence ratio	7
2.4 Flammability limits	7
2.5 Ignition by a point source	7
3 Numerical simulations	11
3.1 Introduction	11
3.2 Governing equations	12
3.3 Initial and boundary conditions	13
3.3.1 The initial temperature distribution	13
3.3.2 Ghost points and boundaries	13
3.3.3 Initial mixture	15
3.4 Energy calculations	15
3.5 The H_2/O_2 reaction mechanism	17
3.6 Hallmarks of ignition	19
4 The method of the simple model	23
4.1 The simple model introduction	23
4.2 Obtaining an expression for the center temperature	24
4.2.1 Assuming that α is constant	26

CONTENTS

4.2.2	Assuming a realistic α which depends on temperature .	26
4.3	The ignition delay time	28
5	Results	31
5.1	Ignition and the spatial design of the heat source	31
5.1.1	The result from the Pencil Code	31
5.1.2	The results from the simple model with different α 's	33
5.1.3	Comparison of the simple model with $\alpha(T_m)$ and the Pencil Code	33
5.2	MIE of the heat source	36
6	Discussion	39
6.1	Ignition and the spatial design of the heat source	39
6.1.1	The Pencil Code	39
6.1.2	The simple model	41
6.2	MIE	43
7	Conclusion	47
	Bibliography	48

List of Figures

2.1	Explosion limits for a H_2/O_2	5
2.2	Different temperature zones in a laminar flame [3]	9
3.1	The initial Gaussian temperature distribution	14
3.2	This figure shows a non ignition case	20
3.3	This figure shows a case of ignition	21
3.4	Time development of the temperature distribution	22
4.1	The thermal diffusivity as a function of temperature	27
4.2	The ignition delay time as a function of the initial temperature	30
5.1	Ignition results from the Pencil Code	32
5.2	Comparison of different results from the simple model	34
5.3	Comparison of the simple model and the Pencil Code	35
5.4	MIE results from the Pencil Code	37
5.5	MIE density from the Pencil Code results	38
6.1	This figure shows how the temperature evolves with time for both the simple model and the Pencil Code	42

List of Tables

2.1	The Flammability Limits for Hydrogen in Air [3]	8
3.1	The hydrogen-oxygen reaction mechanism from Li et al.[5] . .	18
4.1	The parameters from the regression of $\alpha(T)$	28
5.1	MIE's dependency on the heat source radius	36

Chapter 1

Introduction

Knowledge and information about the characteristics of hydrogen combustion are important in a range of applications. Hydrogen gas has many useful properties. It is the lightest gas known and has great buoyancy effects. In addition, it has very good flammable and explosive qualities.

The usage of hydrogen gas in Zeppelins, due to its high buoyancy effect, was well established in the earlier years. However, since the hydrogen molecules are so small, it is a hard gas to contain and leakage can easily occur. This was probably what happened in the Hindenburg disaster, combined with a static discharge an explosion was inevitable. For many industrial processes where hydrogen is involved one has to use extreme caution, and safety issues are very important. As hydrogen has gotten more and more common as fuel in personal vehicles, the general public is forced to indirectly operate hydrogen in their everyday life, and explosion hazard awareness is growing ever more important.

The more that is known about the conditions which are necessary for hydrogen gas to ignite, the easier accidents can be avoided. The developers are then given clearer boundaries and latitudes related to design and safety of hydrogen based products. Furthermore, it will improve the efficiency of hydrogen as a fuel for internal combustion engines.

In this thesis, properties related to the minimum ignition energy (MIE) in a hydrogen combustible mixture are explored. It is done so by numerical simulations in a program called Pencil Code [1]. The main focus is laid down in how the shape of the ignition source affects the MIE. The idea is to imitate an ignition source by a Gaussian temperature distribution and simulate the outcome. The shape of the Gaussian distribution is governed by its height, the center temperature difference, and its width, the standard deviation. By altering these parameters, the ignition results will be affected. If they are chosen carefully, such that the distribution barely gives ignition, one can calculate the energy necessary to obtain this distribution, which would effect

in being the MIE. The Gaussian temperature distribution is

$$T(r) = (T_{\max} - T_0) e^{-\left(\frac{r}{r_{s_0}}\right)^2} + T_0, \quad (1.1)$$

where r_{s_0} is the width and $(T_{\max} - T_0)$ is the height. This will be explored in more detail later on.

In addition to vary the shape of the distribution, ignition simulations will be performed in different dimensions and compared. This provides more information about the heat source. By changing the dimension, one could imagine it being equivalent to changing the geometry of the heat source. For instance, a simulation in two dimensions shows the distribution as a round plate, with its maximum temperature in the center. This could be equivalent of looking at a long cylinder in three dimensions, with a cross section corresponding to the 2D simulations. A different spacial design would be a direct 3D simulation in the form of a sphere.

When numerical simulations are performed in 3D, it is very costly related to computer power. In this thesis a new, less complex, simulation method is proposed with the purpose of replicating the ignition result from the DNS regarding the design of the heat source. In this method many simplifications is done and only the most important physics of the simulation problem are included. This will reduce the cost of computer power, and a balance between accuracy and simplicity are pursued. Furthermore, it will give an insight into the important physics which lies behind.

In addition to this introduction, the thesis consists of six chapters. Firstly it is the theory chapter, which explains some of the properties of ignition and the most important chain reactions in a hydrogen-oxygen system. Furthermore, it states reasons for why there exist explosion and flammability limits. Chapter 3 will deal with the simulation methods of the Pencil Code. Here a basic explanation of how the code works will be given and it will be shown how our problems must be addressed in the simulation program. The next chapter will analyse the procedure of the new, more simplified, simulation method. The assumptions and simplifications in this method will be shown together with how it operates to reproduce the Pencil Code results. The simulation results of both methods will be shown by figures and presented in the result chapter. These results will be further analysed in the discussion chapter, before the most important findings will be stated in the conclusion chapter.

Chapter 2

Theory

2.1 Chain reactions

When hydrogen reacts with oxygen to form water it cannot be described by a single reaction. Even though $2H_2 + O_2 \rightarrow 2H_2O$ is the overall reaction, meaning that it explains the final products that the initial reactants will end up as, it is not sufficient. The process involves a series of intermediate steps which occurs by a chain process and involve many radical species. Radicals can be atoms, molecules or ions that have free unpaired electrons which cause them to be highly reactive. The involved radicals in a hydrogen-oxygen system are the species H , O and OH . In addition, hydroperoxyl, HO_2 , has to be included, but in comparison this radical is relatively stable.

A chain process is divided into different types of chain reactions dependent on their various characteristics. The chain *initiation steps* are accountable for creating the initial radicals which will initiate the chain process. One possibility is when molecular hydrogen dissociates into atomic hydrogen by the reaction



where M denotes any third body species that are not directly involved in the reaction. Dissociation of oxygen would also be possible, but the dissociation energy of oxygen is higher than that of hydrogen. Reaction (2.1) is very endothermic and is only believed to yield for high temperatures. A more proper reaction, (2.2), which is often mentioned in the literature as the main initiation step, provides two radicals for the system, but as mentioned HO_2 is more stable than H , and will not have a major participation in initiating further steps. This reaction is given as



Whether the dominant reaction is (2.1) or (2.2) is not very essential. The

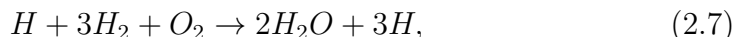
essence lies in that the initiation step provides unstable H atoms that launch a series of reactions.

The important steps are



In this reaction system there are two types of reactions called *chain propagation* and *chain branching*. The difference between the two are seen in that the branching steps produce two or more radicals by the consumption of only one, while the propagation step only reproduces the number of radicals.

If reactions (2.3) to (2.6) are given free hands, there will be an enormous increase in the number of radicals that are been produced. For instance, by combining reaction (2.3), (2.4) and (2.5) as shown in Laidler (1987) [2], we get an overall reaction of



which means that for each cycle one H atom produces three new ones. This will escalate into a chain branching explosion if there is no function for the radicals to be terminated. However, there are certain restrictions which will limit the radical build-up. Dependent on temperature and pressure there will exist termination steps, which cause the radicals to decrease in numbers. Whether a branched chain explosion occurs or not, will then be dependent on the competing reaction rates between chain branching and chain termination.

The reactions which are included and considered for the hydrogen-oxygen system in this work are only the most important ones, chosen for comprehension. The references for these reactions are from "Combustion" by Glassman & Yetter (2008) [3]. For a complete reaction scheme, we would have had to include many more reactions. Two reaction schemes that are frequently used in numerical simulations are the San Diego chemical kinetic mechanism [4] and the Li et al. mechanism [5]. The latter is quoted in Table 3.1.

2.2 Explosion limits and the oxidative characteristics of hydrogen

For any specific fuel-oxidizer mixture there exist explosion limits, which set the boundaries for whether an explosion or ignition will occur or not. These boundaries are temperature and pressure based, and separates the slow reactions from the fast ones. For a gas to explode, very rapid reactions are

2.2. EXPLOSION LIMITS AND THE OXIDATIVE CHARACTERISTICS OF HYDROGEN

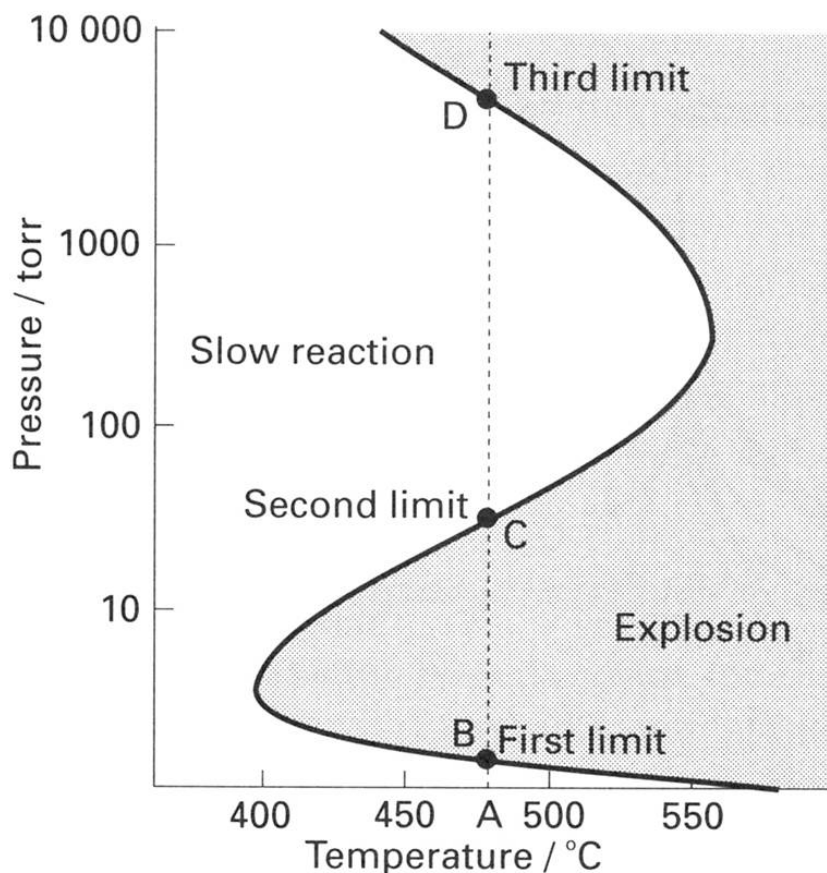


Figure 2.1: Explosion curve for H_2/O_2 and its different limits [6]. The unit torr equals $(1/760)$ atm.

a necessity. The explosion limit curve, Figure (2.1), is divided into different limit zones. To explain them one has to look at the different branched chain mechanisms responsible and how they can be terminated by the *chain termination steps*. There are various mechanisms explaining the limits.

The first limit, separating point A and B in Figure 2.1, can be explained by the following termination steps:



This means that the radicals recombine at the walls to create reactants or products. Since the pressure at the first explosion limit is very low, there are

relatively few molecules in the mixture and fewer reactions will occur. This implies that the size of the containing vessel is of great importance. When the pressure is low the probability that the radicals will make it to the wall and terminate themselves increases. The fact that the first explosion limit depends on the diameter of the vessel has been confirmed by experiments as stated in Glassman & Yetter [3]. If the vessel size is increased this limit would decrease to even lower pressures.

If the pressure is increased, with a constant temperature from the first limit, the system is in the zone between the first and second explosion limit. In this zone the chain branched explosions are possible and will occur. This is because the wall termination steps can no longer compete with the branching steps due to the increased pressure, which causes a decreased probability for radicals to reach the walls. This rapid radical production escalates the number of exothermic reactions happening and an explosion becomes inevitable.

When the pressure is further increased the system again exists in a non-explosion zone, shown in Figure 2.1 as the zone between point C and D. In this region reaction (2.3), which is the most effective branching step, gets overridden by



Reaction (2.11) is a pressure sensitive third-order reaction. In order to form HO_2 by reaction (2.11), and not OH and O as in reaction (2.3), the presence of a third body specie is needed. The concentration of this specie is dependent on the pressure. Higher pressures increase the likelihood for reaction (2.11) instead of (2.3) to occur, which is the main cause for the existence of the second explosion limit. Since HO_2 still keeps its stability it will diffuse to the walls and terminate itself, causing reaction (2.11) to serve as an efficient H radical destroyer.

The third limit can be explained by the change in the HO_2 stability due to an even further increase in pressure. At the third explosion limit, the radical becomes unstable and gets involved in the reaction



which is followed by



The HO_2 molecule then serves as a reactive radical instead of a radical terminator.

Furthermore, if the temperature is above a certain level, a hydrogen combustible mixture will ignite and explode more or less independent of the pressure.

2.3 Stoichiometry and the equivalence ratio

How is the mixture ratio between a specific fuel and the oxygen it is reacting with defined? In order to answer, we need to look at the following definitions, namely stoichiometry and the equivalence ratio.

If we look at the overall chemical reaction for hydrogen and oxygen (2.14) and balance it, the reaction is called stoichiometric, meaning that there are not any hydrogen or oxygen leftovers at the right hand side. This means that if the volume mixture ratio between hydrogen and oxygen is 2:1 the mixture is stoichiometric, and we experience complete combustion.



However this is not always the case. The mixture could be fuel-lean or fuel-rich. *The equivalence ratio* of a system, denoted as ϕ , is the ratio between the actual fuel-oxidizer ratio and the stoichiometric fuel-oxidizer ratio. When $\phi < 1$ the system is fuel-lean or over-oxidized, if $\phi > 1$ the system is fuel-rich and $\phi = 1$ implies that the mixture is stoichiometric. The equivalence ratio is defined to be

$$\phi = \frac{m_{\text{fuel}}/m_{\text{oxy}}}{(m_{\text{fuel}}/m_{\text{oxy}})_{\text{stoich}}} = \frac{n_{\text{fuel}}/n_{\text{oxy}}}{(n_{\text{fuel}}/n_{\text{oxy}})_{\text{stoich}}}, \quad (2.15)$$

where m denotes the mass and n the number of moles.

2.4 Flammability limits

It is obvious that the equivalence ratio of a mixture affects the combustion abilities of the system. Intuition can tell us that in order for combustion to take place, the equivalence ratio cannot be too high or too low. There needs to be a minimum concentration of fuel or oxidizer, in the system for a flame front to propagate.

These limits are called the upper and lower *flammability limit*. They are defined to be the necessary equivalence ratios required for a flame to be self-supported after the ignition source is removed. In other words, the limits denote the very richest and leanest fuel concentrations possible without the flame extinguishing itself. Experimental data of the flammability limits for hydrogen and air mixtures can be seen in Table 2.1.

2.5 Ignition by a point source

An induced spark is the most common way of achieving a forced ignition. It is used in a range of applications, for instance, in the automotive cylinder

Table 2.1: The Flammability Limits for Hydrogen in Air [3]

	Lower(lean)	Upper(Rich)	Stoichiometric
Volume %	4	75	29.2
ϕ	0.1	7	1

inside the engine of a gasoline car. The sparks are often created by two capacitors as an electrical discharge, with spark durations from $0.01\mu\text{s}$ to about $100\mu\text{s}$ for larger engines.

A spark ignition is by Zeldovich approach looked upon as a point source, which releases an amount of heat. The approach followed here are obtained from the ignition chapter in "Combustion" by Glassman et al. [3].

How the heat distribution varies with time can be obtained from the heat equation

$$\frac{\partial T}{\partial t} = \alpha \nabla^2 T, \quad (2.16)$$

where $\alpha = (\lambda/\rho c_p)$ is the thermal diffusivity and λ is the thermal conductivity. Equation (2.16) governs how the temperature distribution diffuses to its surroundings as time evolves. The boundary conditions for equation (2.16) in spherical coordinates are $T(r = \infty) = T_0$ and $(\partial T/\partial r)(r = 0) = 0$.

The input energy for any temperature distribution is given as

$$Q'_v = 4\pi c_p \rho \int_0^\infty (T - T_0) r^2 dr \quad (2.17)$$

which states that at any given time, Q'_v is the energy necessary to obtain the given distribution when no heat is produced in the mixture.

The solution of equation (2.16) will then be

$$T - T_0 = \frac{Q'_v}{c_p \rho (4\pi \alpha t)^{3/2}} e^{-r^2/4\alpha t} \quad (2.18)$$

An expression for the maximum temperature is found when we let $r \rightarrow 0$ and (2.18) becomes

$$T_M - T_0 = \frac{Q'_v}{c_p \rho (4\pi \alpha t)^{3/2}} \quad (2.19)$$

where T_M is the maximum temperature in the distribution.

The condition for ignition is when the characteristic cooling time τ_c is larger than the reaction time τ_r . The cooling time is associated with the

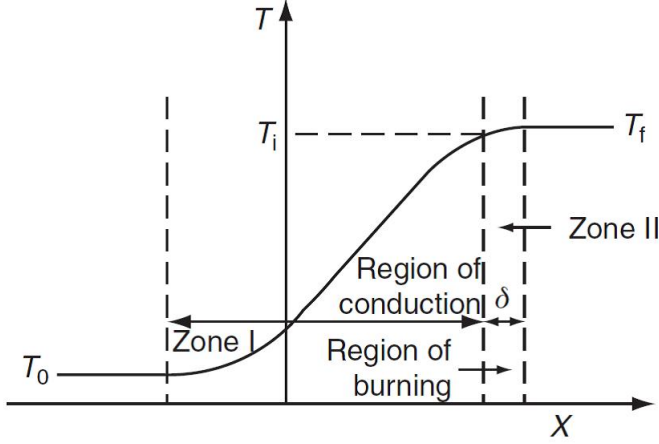


Figure 2.2: Different temperature zones in a laminar flame [3]

period the temperature T_M , at $r = 0$, changes by a value θ . This small temperature change is taken as

$$\theta = \frac{RT_M^2}{E}, \quad (2.20)$$

where R is the universal gas constant and E is the activation energy. How θ is obtained are not shown here, but can be read in the ignition chapter in Glassman et al. [3]. To a close approximation, the characteristic cooling time can be given as

$$\tau_c = \frac{\theta}{\frac{dT_M}{dt}}. \quad (2.21)$$

Considering the input energy for heating a spherical volume with radius r_f from T_0 to T_f uniformly, equation (2.17) becomes

$$Q'_v = \frac{4}{3}\pi r_f^3 c_p \rho (T_f - T_0), \quad (2.22)$$

which leads to an expression for the characteristic cooling time

$$\tau_c = 0.14 \frac{\theta}{T_f - T_0} \frac{r_f^2}{\alpha}. \quad (2.23)$$

When the activation energy is sufficiently large, most of the energy release will be close to the flame temperature, T_f . Thus, the ignition temperature T_i , will be close to T_f . This means that the reaction zone, δ , will be a very small region. In Glassman et al. [3] the reaction time τ_r , which correspond to the reaction zone δ , is expressed with θ by saying that this small temperature

difference is close to $(T_f - T_i)$ as in the Zeldovich-Frank-Kamenetskii-Semenov flame theory. The characteristic reaction time can then be approximated as

$$\tau_r \simeq 2 \frac{\theta}{T_f - T_0} \frac{\alpha}{S_L^2} \quad (2.24)$$

where S_L is the laminar flame speed and $a = \alpha/S_L$ is the thermal width of the flame.

By considering the condition $\tau_c \geq \tau_r$, it can be shown that

$$r_f \geq 3.7a, \quad (2.25)$$

which means that in order to get an ignition, we need a source radius which is greater than the characteristic width of the laminar flame zone. With this condition satisfied the nearby layers of the initial heat source will ignite before the volume of the heat source cools.

Chapter 3

Numerical simulations

The minimum ignition energy for a combustible hydrogen mixture is found by running a series of Direct Numerical Simulations (DNS) with the Pencil Code.

3.1 Introduction

DNS is short for Direct Numerical Simulation, and unlike Large Eddy Simulations (LES) and Reynold-average Navier-Stokes simulations (RANS), which use turbulent modelling, DNS solves the full Navier-Stokes equations numerically without the use of any modelling and filtering. This does not include the approximations done for the discretization of the relevant equations which is the essence in any numerical method. For the time discretization the Pencil Code uses a third order Runge-Kutta method and a sixth-order central difference method is used in space.

The name pencil has its origin in that the Pencil Code uses a one dimensional array of data to calculate the entire time step within the numerical grid instead of operating with large three dimensional arrays. The main advantage of this method is that one allows an entire pencil to be stored in the CPU's cache without detouring it to the much slower random access memory. This improves the efficiency of the code considerably when we are dealing with more modern microprocessors. In some cases, the efficiency has been shown to improve by about 60 percent. [7]

Another treat of the Pencil Code is that it is module based, which makes it easier to customize the code for specific problems. Typical modules are gravity, chemistry, viscosity or entropy, which can be included, excluded or combined together in the code to form the physical properties desired. In addition to these physical modules, there are also technical ones. For instance the message passing interface (MPI) is a module which allows the usage of

multiple CPU's.

The Pencil Code is programmed in FORTRAN and should be compatible with the fortran90 standard and can be used on any UNIX/Linux based system. The Pencil Code is free software which can be obtained from the Pencil Code website [1].

In order to visualize the results obtained from the Pencil Code, a pleasant supplement is the commercial software, IDL, in which the Pencil Code has full compatibility with.

3.2 Governing equations

To simulate a physical problem the Pencil Code has to solve a set of equations dependent on which modules are necessary to include. In our case, we need to solve the conservation equations for mass, momentum, species and energy, together with the equation of state.

The equation for conservation of mass is given as

$$\frac{\partial \ln \rho}{\partial t} + (\mathbf{U} \cdot \nabla) \ln \rho = -\nabla \cdot \mathbf{U}, \quad (3.1)$$

where \mathbf{U} is the velocity vector and ρ the density. The momentum equation has the form

$$\frac{\partial \mathbf{U}}{\partial t} + (\mathbf{U} \cdot \nabla) \mathbf{U} = \frac{1}{\rho} (-\nabla p + \mathbf{F}_{vs}) + \mathbf{f}, \quad (3.2)$$

where \mathbf{F}_{vs} is the viscous force, p is the pressure and \mathbf{f} is any type of external forces, e.g. gravity. The conservation law of the species is written as

$$\rho \frac{\partial Y_j}{\partial t} + \rho (\mathbf{U} \cdot \nabla) Y_j = -\nabla \cdot \mathbf{J}_j + \dot{\omega}_j, \quad (3.3)$$

where $\dot{\omega}_j$ is the reaction rate, \mathbf{J}_j is the diffusive flux and Y_j is the mass fraction. The j 's denote the different species. Lastly, the energy equation is listed as

$$\left(c_p - \frac{R}{M} \right) \frac{D \ln T}{Dt} = \sum_j \frac{D Y_j}{Dt} \left(\frac{R}{M_j} - \frac{h_j}{T} \right) - \frac{R}{M} \nabla \cdot \mathbf{U} + \frac{2\nu \mathbf{S}^2}{T} - \frac{\nabla \cdot \mathbf{q}}{\rho T}, \quad (3.4)$$

where c_p is the heat capacity at constant pressure, R is the universal gas constant, M is the molar mass, T is the temperature, h is the enthalpy, \mathbf{q} is the heat flux and $D/Dt = \partial/\partial t + \mathbf{U} \cdot \nabla$.

For a more thorough discussion on the equations solved in the Pencil Code, see Babkovskaia, Haugen and Brandenburg (2010) [8].

3.3 Initial and boundary conditions

3.3.1 The initial temperature distribution

To simulate an ignition source in the Pencil Code an initial temperature distribution is inserted into the domain. The distribution is chosen to be Gaussian, and parallels could be drawn to a real life heat source that has its hottest spot in the center. For instance, if a cross-section of a real electrical spark is made, the temperature distribution at this cross-section could compare well with a Gaussian shaped temperature distribution in two dimensions. The initial distribution is given by (1.1)

$$T(r) = (T_{\max} - T_0) e^{-\left(\frac{r}{r_{s0}}\right)^2} + T_0, \quad (3.5)$$

where T_{\max} is the maximum temperature, T_0 is the temperature of the surroundings and r_{s0} is the radius of the distribution. Since the factor of $1/2$ is not included in the exponent of the exponential function in equation (3.5), the standard deviation is $\sqrt{2}r_{s0}$. Figure 3.3.1 illustrates the different variables and for a one dimensional simulation this is how the distribution would look like. For the two dimensional simulations the same distribution is used, only that it is rotated in the plane and has its maximum temperature in the center. If one expresses the 2D distribution in terms of polar coordinates, it would have a constant temperature at any given r for all θ . In other words, the distribution has circular symmetry. The same goes for the 3D simulations, they are chosen to have spherical symmetry.

3.3.2 Ghost points and boundaries

To implement boundaries for a sixth-order difference scheme in space, we need something called ghost points. These are points outside the grid where no equations are solved, but they are used for calculations at the boundaries. In order to calculate a value of a point on the domain, the values of the six closest points in each dimension is needed when dealing with a sixth order method in space. At the boundaries, it is then necessary to include three points outside the domain. If n_x is the number of grid points in the x-direction of the domain, the total number of points in the applicable array would be $n_x + 6$.

The values of the ghost points can be instructed to be periodic, symmetric or asymmetric relative to the grid points. Asymmetric ghost points imply zero values at the boundary, while symmetric ghost points imply zero first derivatives. In the periodic condition the ghost points are given the values of the three closest points to the boundary at the opposite end of the array.

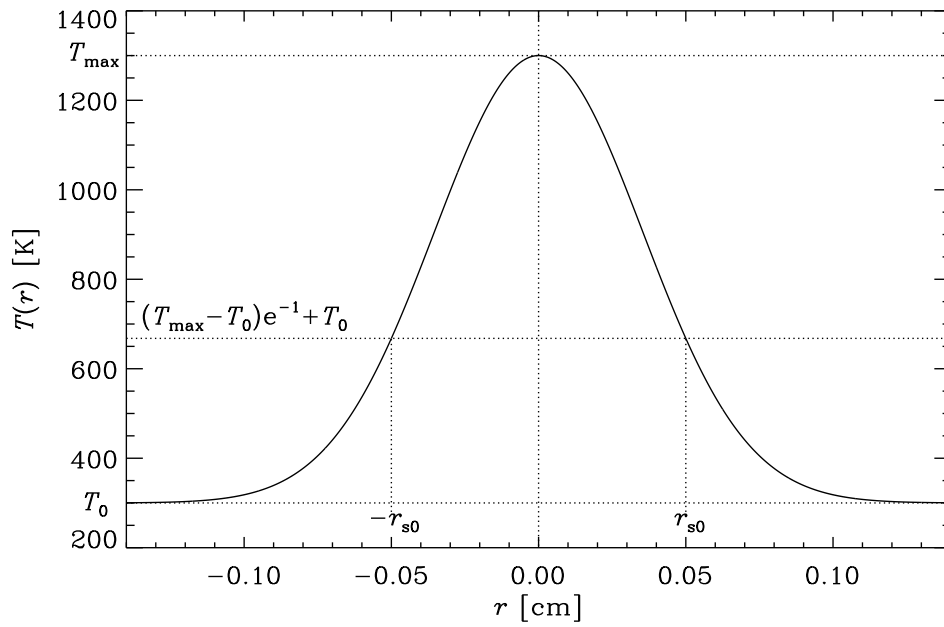


Figure 3.1: Illustration of the initial Gaussian temperature distribution, where $T_0 = 300$ K, $r_{s0} = 0.05$ cm and $T_{\max} = 1300$ K. The value $(T_{\max} - T_0)e^{-1} + T_0$ denotes the temperature at r_{s0} .

To simulate a closed vessel or container, we need to stage the ghost points in such a way that the boundaries act like walls. Therefore, the velocity components are set to asymmetric, since the velocity at the walls must be zero. The other components such as temperature, pressure, mass fraction of the species and density must have a zero first derivatives at the walls and need symmetric ghost points. The domain is chosen to be sufficiently large, which implies that $\frac{\partial T}{\partial r}(r = r_{\max}) = 0$.

3.3.3 Initial mixture

The flammable gas we want to simulate is dry air mixed with hydrogen, so the initial species are H_2 , O_2 and N_2 . We have assumed that all the minor species in the air, such as argon and carbon-dioxide are negligible and that the initial gas is completely homogeneous. The air is set to consist of 79% nitrogen and 21% oxygen when measured in volume percentage. This volume percentage ratio is set to persist when hydrogen is included into the mixture.

The overall reaction of hydrogen and air can be written as



where $a = \frac{1}{2\phi}$ and equal to 1/2 if the mixture is stoichiometric. For a desired equivalence ratio, the initial volume and mass fractions of the system can be calculated.

The radicals are not included in the initial mixture, even though the temperature profile already exists in the system at time zero. The radicals will start to form immediately after the simulation is started.

3.4 Energy calculations

The energy required is the input energy necessary to obtain a initial temperature distribution. To show how the energy could be calculated, the easiest is to consider the one dimensional case. It is here shown analytically for illustration purposes.

By transforming equation (2.17) to yield for one dimension the input energy, in the form of heat, is given as

$$Q = 2 \int_0^\infty c_p(T(r)) \cdot \rho(T(r)) \cdot (T(r) - T_0) dr, \quad (3.7)$$

where Q is the input energy per unit area and $T(r)$ is the initial temperature distribution as given in equation (3.5). The expression for the density as a function of temperature can be found by the use of the ideal gas law,

$P = \frac{\rho RT}{M}$, with the pressure, P , and the mean molar mass, M , held constant. The density is then given as

$$\rho(T(r)) \cdot T(r) = \rho_0 \cdot T_0. \quad (3.8)$$

where ρ_0 and T_0 are the ambient values. Inserting equation (3.5) into equation (3.7) and (3.8), and then combine the last two, it yields

$$Q = 2\rho_0 T_0 \int_0^{L_x} c_p(T(r)) \frac{(T_{\max} - T_0) e^{-\left(\frac{r}{r_{s0}}\right)^2}}{(T_{\max} - T_0) e^{-\left(\frac{r}{r_{s0}}\right)^2} + T_0} dr, \quad (3.9)$$

where L_x is the length of the domain. A simplification of the specific heat would be to average it in the following way,

$$c_p(T(r)) \simeq \bar{c}_p = \frac{c_p(T_{\max}) + c_p(T_0)}{2}, \quad (3.10)$$

which is done here to simplify the illustration. It is now possible to calculate equation (3.9), with a numerical solver, for a given set of r_{s0} and T_{\max} .

Strictly speaking, the specific heat should be calculated as a polynomial function of temperature, where the constants are obtained from thermodynamical tables. Then the calculations of the input energy would be more accurate.

In this thesis the energy is actually obtained numerically in the Pencil Code, and the method above was showed to make the energy calculation more comprehensible. How it is done in Pencil Code is by instructing the program to calculate the energy for each grid point and then take the sum over the domain. The ambient temperature is subtracted from the temperature distribution to give the excess energy in each point. This can, for one dimension, be illustrated as

$$Q = \sum_{i=1}^{n_x} c_{p_i} \rho_i (T_i - T_0) \Delta x \quad (3.11)$$

where n_x is the number of grid points along the x-direction, i denotes the different grid points and Δx is the spacing between them when an equidistant grid is assumed.

When comparing the energy calculations from equation (3.9) with \bar{c}_p , and the calculations from equation (3.11) done in the Pencil Code, they differ from each other by about (1 – 3)%. This error is mainly due to the averaged specific heat in equation (3.9). In the Pencil Code c_p is calculated along the grid points based on the current temperature at each point, while in equation (3.11) the specific heat is only averaged between T_m and T_0 .

3.5 The H_2/O_2 reaction mechanism

The reaction mechanism used for hydrogen-oxygen combustion is the Li et al. mechanism [5]. The mechanism is shown in Table 3.1 and involves 19 reactions. This is a complicated process, but compared to combustible systems containing hydrocarbons it is a rather simple mechanism. The most important reactions are covered in chapter 2.

Table 3.1: The hydrogen-oxygen reaction mechanism from Li et al.[5]

No.	Reaction
	<i>H₂/O₂ chain reaction</i>
R1	$H + O_2 = O + OH$
R2	$O + H_2 = H + OH$
R3	$H_2 + OH = H_2O + H$
R4	$O + H_2O = OH + OH$
	<i>H₂/O₂ dissociation/recombination reaction</i>
R5	$H_2 + M = H + H + M$
R6	$O + O + M = O_2 + M$
R7	$O + H + M = OH + M$
R8	$H + OH + M = H_2O + M$
	<i>Formation and consumption of HO₂</i>
R9	$H + O_2 + M = HO_2 + M$
R10	$HO_2 + H = H_2 + O_2$
R11	$HO_2 + H = OH + OH$
R12	$HO_2 + O = O_2 + OH$
R13	$HO_2 + OH = H_2O + O_2$
	<i>Formation and consumption of H₂O₂</i>
R14	$HO_2 + HO_2 = H_2O_2 + O_2$
R15	$H_2O_2 + M = OH + OH + M$
R16	$H_2O_2 + H = H_2O + OH$
R17	$H_2O_2 + H = HO_2 + H_2$
R18	$H_2O_2 + O = OH + HO_2$
R19	$H_2O_2 + OH = HO_2 + H_2O$

3.6 Hallmarks of ignition

The Figures, 3.2 and 3.3, show the time development of two different simulations. Seven of the graphs indicate how the distinctive mass fractions develop, where the last one shows how the maximum temperature, $T_m(t)$, changes through time. The two simulations have identical initial conditions, except for the width, r_{s_0} , which differs by 0.001 cm. Although the difference is small, the simulation represented in Figure 3.3, with $r_{s_0} = 0.028$ cm, ignites, while the other simulation shown in Figure 3.2, with $r_{s_0} = 0.0279$ cm, does not. By comparing the two figures, a clear distinction between them can be seen, in that something drastic happens after about 0.2 ms in Figure 3.3. After this point there is a sudden increase in temperature, a large radical build-up and the mass fraction of the reactants are dropping. Furthermore, the end product, H_2O , starts to form quicker and increases its concentration. All these signs are characteristics of an ignition. In Figure 3.2 we see that the mass fraction of hydrogen gas, H_2 , is almost constant, the radicals appear in very small concentrations and the temperature is dropping at a steady rate due to heat diffusion. Please note that the mass fraction scales in the two figures, concerning H , O and OH in particular, are very different.

These two simulations are chosen to illustrate how a case of ignition is determined and separated from a non ignition case. To find and determine the exact temperature profile necessary for ignition, one has to do a number of simulations per set of initial conditions. For instance, T_{\max} is, for each simulation, varied until the exact height of the temperature distribution for an ignition is found, with r_{s_0} and other parameters held constant. Then the temperature profile is minimized to barely give ignition, which means that the energy it corresponds to will be the minimum ignition energy.

An interesting side notice here is the fact that the radicals HO_2 and H_2O_2 in Figure 3.3 have a sudden increase and decrease in their mass fractions at the time of ignition. Since our simulations are done with a pressure of 1 atm we find ourselves in the region of the third explosion limit. In this region the stability of HO_2 ceases and reaction (2.12) starts to form H_2O_2 radicals.

Figure 3.4 demonstrates how the whole temperature distribution develops in time when an ignition is eminent. It is taken from the same simulation in which Figure 3.3 was based on. The first panel, 3.4(a), shows the initial temperature distribution at time zero. Here one can notice the initial conditions $r_{s_0} = 0.028$ cm, $T_{\max} = 1300$ K and the typical Gaussian shape.

The second panel 3.4(b) is captured at the time where $T_m(t)$ has its lowest value. It can be seen that the distribution is more lubricated than in the previous panel. This is because the temperature has diffused to its surroundings and the mixture has not yet had time to start to produce heat. Up to this point, the heat diffusion has been greater than the heat generation

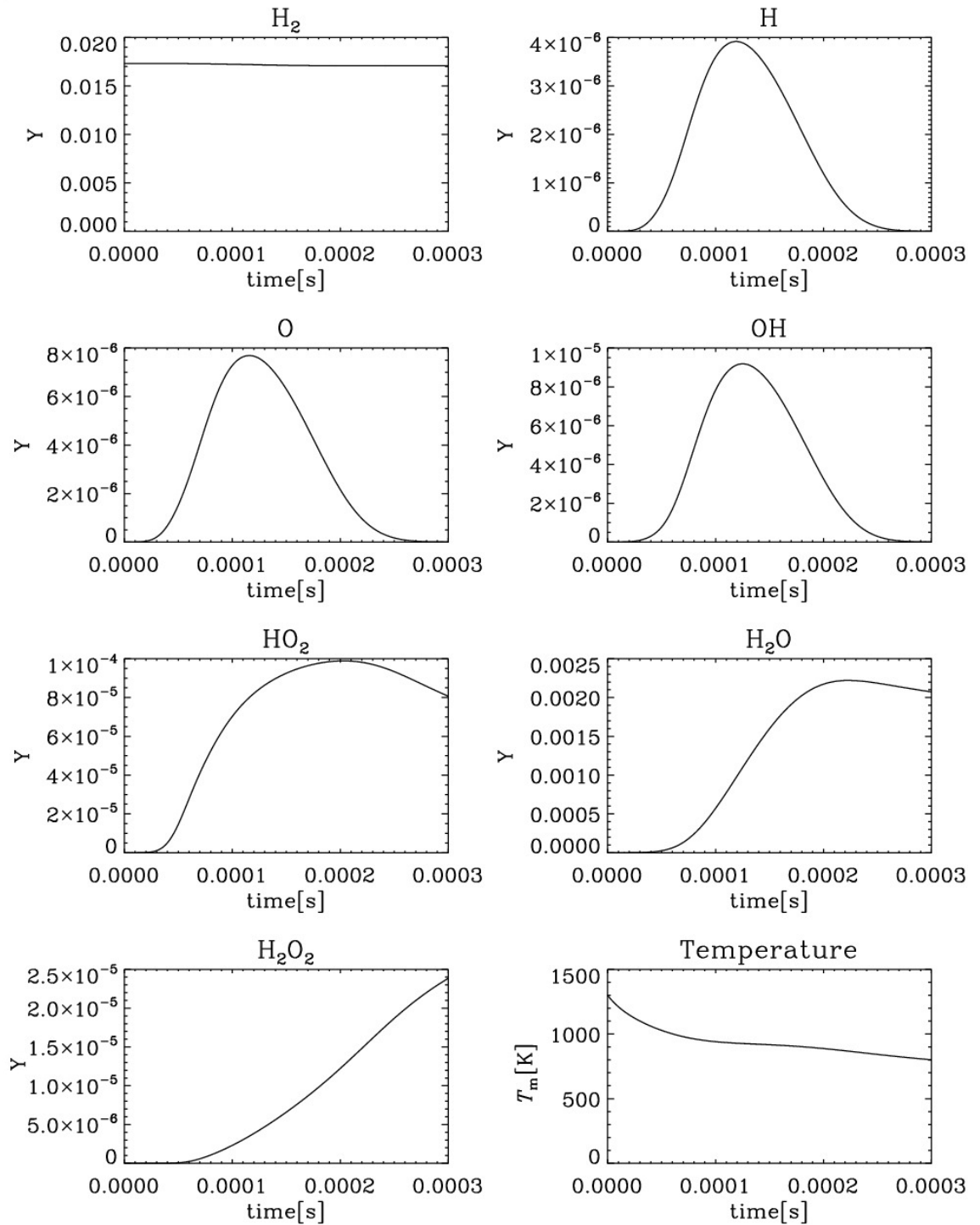


Figure 3.2: This figure shows a non ignition case. It is a 1D simulation with the initial conditions $\phi = 0.6$, $T_{\max} = 1300$ K, $T_0 = 298$ K, $P_0 = 1$ atm and $r_{s_0} = 0.0279$ cm. The mass fractions are denoted as Y .

3.6. HALLMARKS OF IGNITION

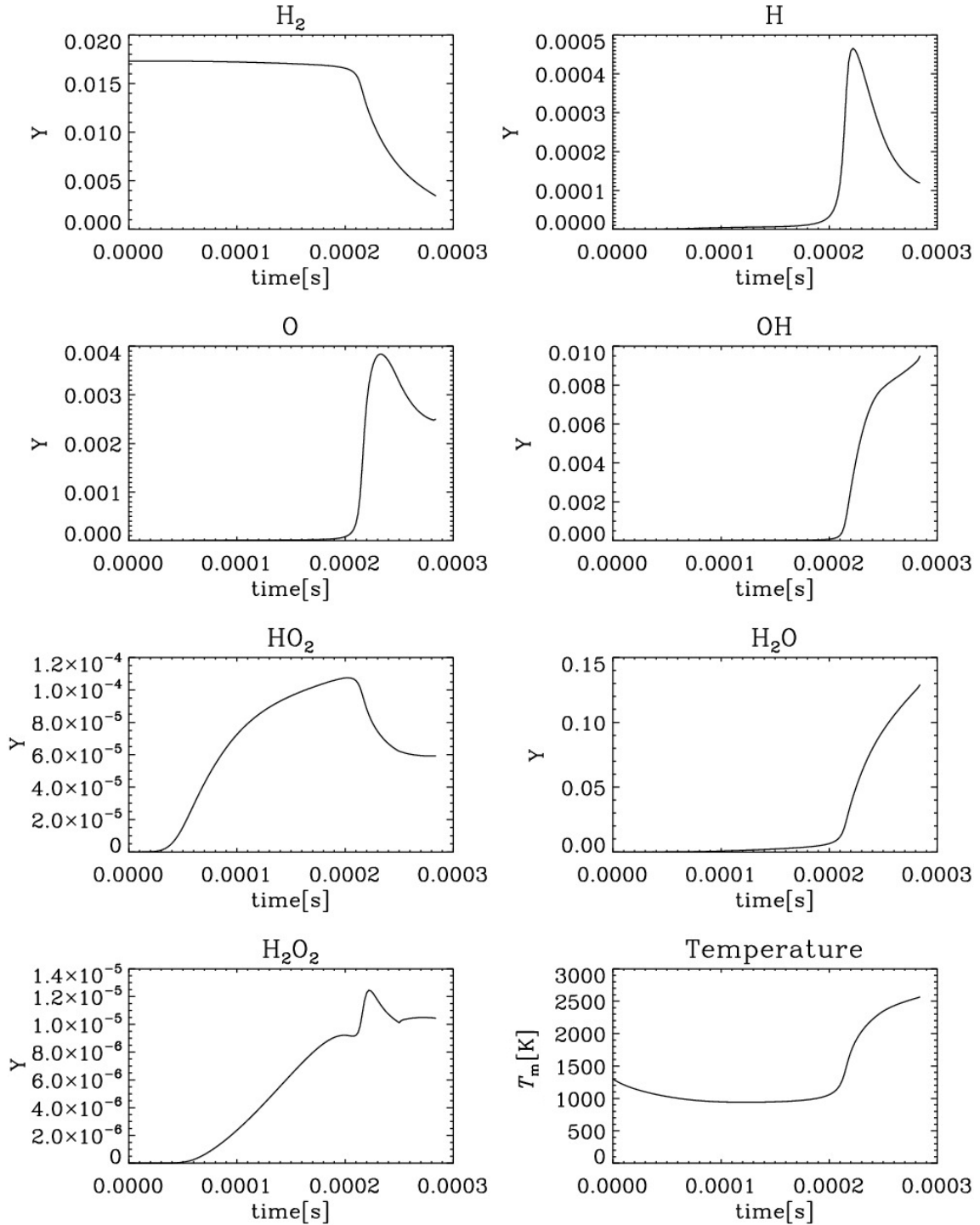


Figure 3.3: This figure shows a case of ignition. It is a 1D simulation with the initial conditions $\phi = 0.6$, $T_{\max} = 1300$ K, $T_0 = 298$ K, $P_0 = 1$ atm and $r_{s_0} = 0.028$ cm. The mass fractions are denoted as Y .

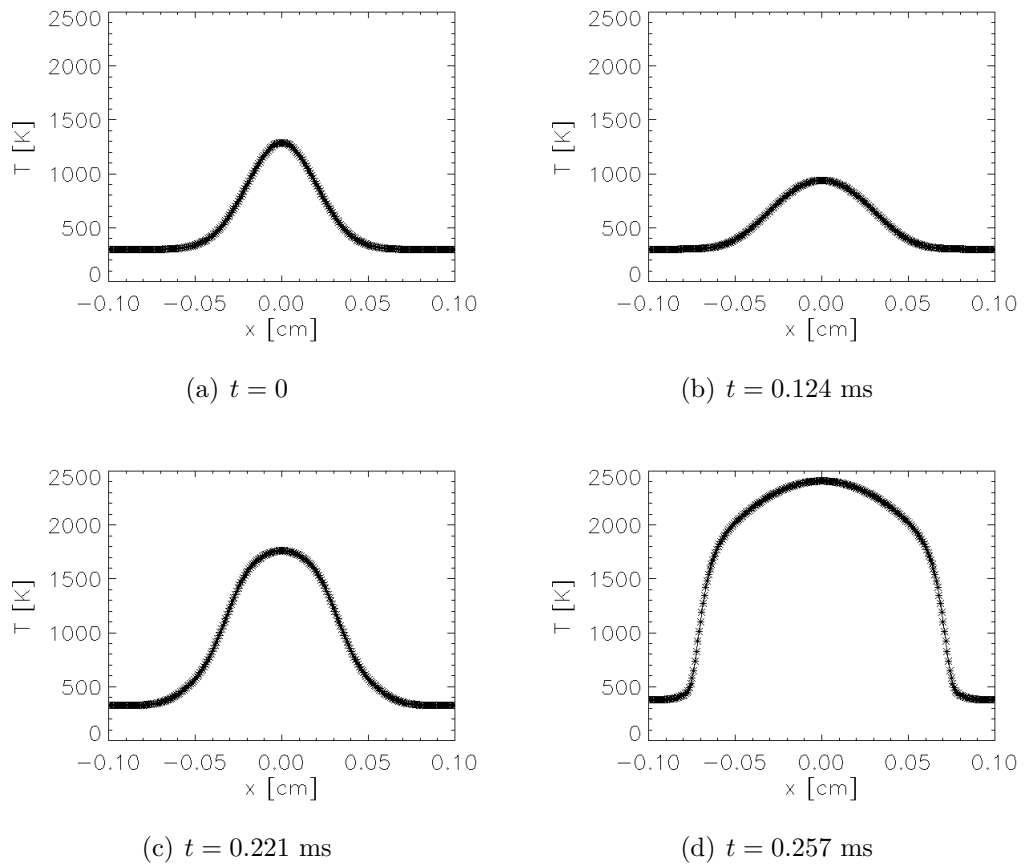


Figure 3.4: The panels show the time development of the temperature distribution for Figure 3.3.

caused by the branched chain reactions, and the temperature is now at the turning point, where it starts to rise.

The next two panels, 3.4(c) and 3.4(d), show that heat is rapidly being produced and that the temperature is rising fast. From panel 3.4(d) it is clear that an ignition has taken place and the flame front on each side of the origin is noticeable.

Chapter 4

The method of the simple model

4.1 The simple model introduction

The purpose of this ignition model is mainly to involve less calculation power than what the Pencil Code simulations need and still be able to determine the temperatures and radii necessary for a potential heat source in a combustible mixture to ignite. This would in particular show its usage if the model could reproduce the results done by Pencil Code in 3D, since these simulations require most computation time. In the following the model is referred to as just the simple model.

The main simplifications done in the simple model are, that it does not directly include chemistry, and that it only calculates the temperature in one point. The temperature is calculated at the point where $r = 0$.

Chemistry is required for the ability to predict properties about ignition. Therefore, chemistry also needs to be accounted for in the simple model, but here it is done in an indirect manner. The model bases its existence on information about the ignition delay time, τ_{ig} , for a given mixture. The ignition delay time is usually given as a function of temperature, as seen in Figure (4.2), and when transferred into this model and used correctly, it should provide the simple model with the necessary information needed in order to replace the direct chemical calculations.

Even though the calculations in this model only involves one single point, it is still desirable to include diffusion of heat as time evolves. This is done by evaluating the appropriate equations at $r = 0$ after the connection between the heat equation and the temperature distribution has been made. Since the simple model assumes a Gaussian temperature distribution, which is symmetric around $r = 0$, the model will probe the maximum center temperature,

$T_m(t)$, at any given time.

In the following sections it will be shown how the Gaussian temperature distribution and the heat equation are connected to form an expression of the center temperature as a function of time. Furthermore, it will be illustrated how this expression gets connected with the ignition delay time, and how the simple model determines a case of ignition. Hydrogen will be used as the combustible fuel in the sense that the ignition delay time data is from a hydrogen-air mixture.

By setting the system properties, as temperature distribution and equivalence ratio in the simple model, equal to how it is set in Pencil Code, the condition for reproducing the results from Pencil Code should be present.

4.2 Obtaining an expression for the center temperature

The Gaussian temperature distribution has the following shape when the time dependency is included

$$T(r, t) = (T_m(t) - T_0) e^{-\left(\frac{r}{r_s(t)}\right)^2} + T_0, \quad (4.1)$$

where T_0 is the ambient temperature, $T_m(t)$ the maximum temperature and $r_s(t)$ is the radius of the heat source, in this case the standard deviation. The initial values at $t = 0$ are defined to be

$$T_m(0) = T_{\max} \quad (4.2)$$

$$r_s(0) = r_{s0}. \quad (4.3)$$

The heat equation is needed in this model in order to include heat diffusion, and is given as

$$\frac{\partial T}{\partial t} = \alpha \nabla^2 T, \quad (4.4)$$

where α is the thermal diffusivity. In 2D, it is convenient to use the polar coordinate system, and in 3D it is the spherical coordinate system which is the most convenient one. Since both θ and ϕ are set to be symmetric, the derivatives with respect to θ and ϕ will be zero in our system. Hence, the Laplace operator here is only given with its r – terms:

$$\nabla^2 = \frac{\partial^2}{\partial r^2}, \quad \text{1D} \quad (4.5)$$

$$\nabla^2 = \frac{1}{r} \frac{\partial}{\partial r} \left(r \frac{\partial}{\partial r} \right), \quad \text{2D} \quad (4.6)$$

$$\nabla^2 = \frac{1}{r^2} \frac{\partial}{\partial r} \left(r^2 \frac{\partial}{\partial r} \right). \quad \text{3D} \quad (4.7)$$

4.2. OBTAINING AN EXPRESSION FOR THE CENTER TEMPERATURE

By inserting the Gaussian temperature distribution, equation (4.1), into the heat equation, equation (4.4), and then evaluate the remaining equation at $r = 0$

$$\left. \frac{\partial}{\partial t} T(r, t) \right|_{r=0} = \alpha \nabla^2 \left((T_m(t) - T_0) e^{-\left(\frac{r}{r_s(t)}\right)^2} + T_0 \right) \Big|_{r=0}, \quad (4.8)$$

it simplifies to

$$\frac{\partial T_m(t)}{\partial t} = -2\alpha N \frac{T_m(t) - T_0}{r_s(t)^2}, \quad (4.9)$$

where $N = 1, 2, 3$ is the number of dimensions.

Since equation (4.9) has two variables that depend on time, $T_m(t)$ and $r_s(t)$, an additional relation between them is needed in order to solve the problem. A relation could be obtained by stating that the area under the Gaussian curve is constant at any given time as heat diffuses. In the three different dimensions this condition can be written as

$$2 \int_0^{\infty} (T(r, t) - T_0) dr = \text{constant}, \quad (4.10)$$

$$2\pi \int_0^{\infty} (T(r, t) - T_0) r dr = \text{constant}, \quad (4.11)$$

and

$$4\pi \int_0^{\infty} (T(r, t) - T_0) r^2 dr = \text{constant}, \quad (4.12)$$

for the 1D, 2D and 3D cases, respectively. Equation (4.10) is similar to equation (3.7), but here c_p and ρ are taken as constants to simplify equation (4.17). By inserting equation (4.1) into (4.10), (4.11) and (4.12) the integrals become

$$2 \int_0^{\infty} (T_m(t) - T_0) e^{-\frac{r^2}{r_s(t)^2}} dr = \sqrt{\pi} \cdot ((T_m(t) - T_0) \cdot r_s(t)), \quad (4.13)$$

$$2\pi \int_0^{\infty} (T_m(t) - T_0) r e^{-\frac{r^2}{r_s(t)^2}} dr = \pi \cdot ((T_m(t) - T_0) \cdot r_s^2(t)), \quad (4.14)$$

$$4\pi \int_0^{\infty} (T_m(t) - T_0) r^2 e^{-\frac{r^2}{r_s(t)^2}} dr = \pi^{3/2} \cdot ((T_m(t) - T_0) \cdot r_s^3(t)). \quad (4.15)$$

Since the integrals are constant, the initial conditions (4.2) and (4.3) can be used as follows

$$\pi^{N/2} \cdot (T_m(t) - T_0) \cdot r_s(t)^N = \pi^{N/2} \cdot (T_{\max} - T_0) \cdot r_{s_0}^N. \quad (4.16)$$

From this equation $r_s(t)$ can be solved for, and the expression simplifies to

$$r_s(t) = r_{s_0} \left(\frac{T_{\max} - T_0}{T_m(t) - T_0} \right)^{\frac{1}{N}}, \quad (4.17)$$

where N again is the number of dimensions. The variable $r_s(t)$ can now be replaced in equation (4.9) to obtain a solvable first order differential equation, which is given as

$$\frac{\partial T_m(t)}{\partial t} = -2\alpha N \frac{(T_m(t) - T_0)^{\frac{2+N}{N}}}{r_{s_0}^2 (T_{\max} - T_0)^{\frac{2}{N}}}. \quad (4.18)$$

The problem that remains is how to treat the thermal diffusivity.

4.2.1 Assuming that α is constant

When it is assumed that α is constant, equation (4.18) can be solved analytically with the initial condition (4.2), to form the following expression

$$T_m(t) = r_{s_0}^N \frac{(T_{\max} - T_0)}{(4\alpha t + r_{s_0}^2)^{\frac{N}{2}}} + T_0. \quad (4.19)$$

Then by inserting equation (4.19) into equation (4.17), $r_s(t)$ is found to be

$$r_s(t) = \sqrt{r_{s_0}^2 + 4\alpha t}. \quad (4.20)$$

To assume that α is constant is not a very correct assumption, but it is done in an attempt to make the simple model as simple as possible and indeed the expressions get simpler. Furthermore, it would limit the amount of external information one would need.

4.2.2 Assuming a realistic α which depends on temperature

A more correct way to solve equation (4.18) is to use a thermal diffusivity which depends on temperature. The thermal diffusivity, α , is given in terms

4.2. OBTAINING AN EXPRESSION FOR THE CENTER TEMPERATURE

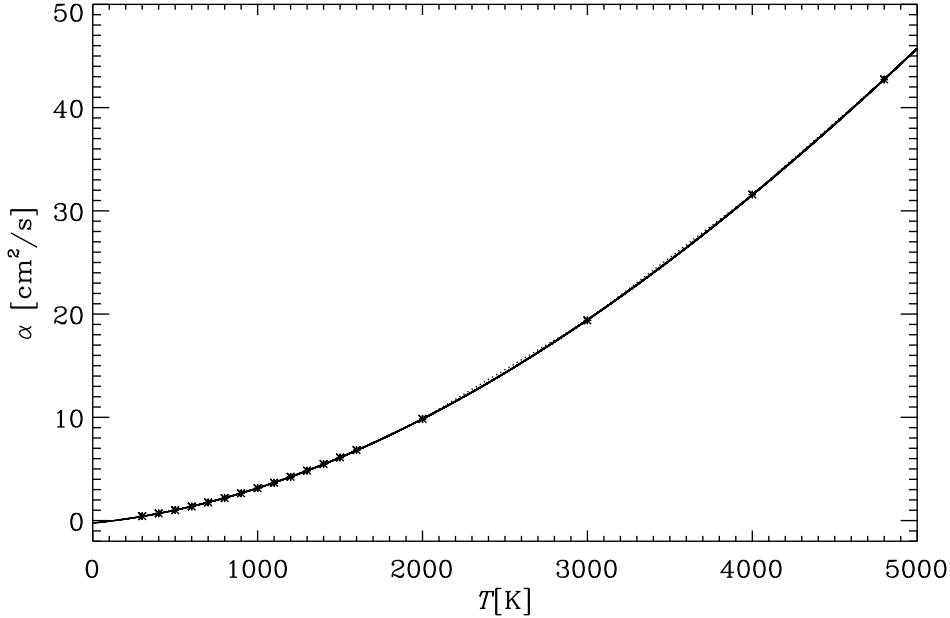


Figure 4.1: Shows the thermal diffusivity as a function of temperature in a hydrogen-air mixture. The dots are the data values obtained from the Pencil Code, and the solid line is the fitted function curve.

of the thermal conductivity, λ , the specific heat with constant pressure, c_p , and the density, ρ , in the following way

$$\alpha = \frac{\lambda}{c_p \rho}. \quad (4.21)$$

Figure 4.1 shows data points of α , obtained from the Pencil Code, as a function of temperature. To obtain a function for the thermal diffusivity based on the data points, regression is used. A function which accounts well is a fourth order polynomial on the form

$$\alpha(T_m(t)) = \left(E + DT_m(t) + CT_m^2(t) + BT_m^3(t) + AT_m^4(t) \right). \quad (4.22)$$

The parameters from the regression are given in Table 4.1.

Equation (4.18) now looks like

$$\frac{\partial T_m(t)}{\partial t} = -\alpha(T_m(t)) \frac{2N}{r_{s_0}^2} \cdot \frac{(T_m(t) - T_0)^{\frac{2+N}{N}}}{(T_{\max} - T_0)^{\frac{2}{N}}}, \quad (4.23)$$

which is a difficult equation to solve analytically. To solve this differential equation, a numerical fourth order Runge-Kutta method is used.

Table 4.1: The parameters from the regression of $\alpha(T)$

Parameter	Value
A	$0.133608 \cdot 10^{-13}$
B	$0.208675 \cdot 10^{-9}$
C	$0.234699 \cdot 10^{-5}$
D	$0.971533 \cdot 10^{-3}$
E	$0.257533 \cdot 10^{-5}$

4.3 The ignition delay time

Until now, the physical elements included in the model do not involve any chemistry. To account for all the chemistry involved in an ignition process the ignition delay time is used.

The typical way to address data about the ignition delay time, τ_{ig} , in the literature, is by plots of how τ_{ig} depends on temperature. Usually the horizontal axis is then given as the inverse initial temperature and the vertical axis by the logarithm of the ignition delay time, see Figure 4.2.

For the simple model to be able to predict ignition in a given mixture, one need to obtain data on the ignition delay time from that specific mixture. In this case the mixture is that of hydrogen-air, with an equivalence ratio of 0.8.

In order to measure the ignition delay time, one needs a definition of when an ignition has taken place. In other words, the ignition delay time must be defined, and there are two common ways of doing that. The first definition is that τ_{ig} is measured until the current temperature has increased 400 K past the initial temperature and the second one defines it to be the time it takes before the derivative of the temperature, with respect to time, is at its highest.

Figure 4.2 shows how the ignition delay time depends on temperature. In the figure there are three data sets, one is from Zhao et al. (2010) [9], and the other two are obtained from simulations with the Pencil Code. The results from Zhao et al. is based on a stoichiometric hydrogen-air mixture and the two results from the Pencil Code is for an equivalence ratio of 0.8. The fact that the results from Zhao et al. shows a minor deviation, could be explained in that the equivalence ratio is different.

The two ignition delay time results from the Pencil Code, which is based on the two different methods of ignition determination, differs when the temperature gets sufficiently high. For such high temperatures the first definition

is the weakest one because there seems to be an upper limit of how high the temperature in the mixture can get. At some point the mixture will not exceed 400 K above the initial temperature and τ_{ig} increases very rapid. This tendency can be seen from the figure, and the regression line is calculated based on the second ignition method for high temperatures.

The ignition delay time results from the Pencil Code are obtain by doing a zero dimensional simulation, and since the ignition delay time should be measured for a uniform temperature, there are no need for a spacial grid. This will effectively reduce the calculation time and a result from a higher dimensional simulation with a homogeneous temperature and mixture would produce the same result. For these simulations a Runge-Kutta-Fehlberg method is used for the time discretization.

The reason why regression is done, is because the ignition delay time is needed as a function of temperature, $\tau_{\text{ig}}(T)$, in order to relate the data from Figure 4.2 to equation (4.18) and (4.24).

The goal of the simple model is to use $\tau_{\text{ig}}(T)$ together with the Gaussian temperature distribution and the heat equation, and then predict, based on the initial parameters T_{max} and r_{s0} , if the mixture ignites or not. Until now, it has been shown that the ignition delay time can be connected to the temperature $T_{\text{m}}(t)$, but to decide if a gas ignites an additional condition is needed. This condition would also need to relate $\tau_{\text{ig}}(T)$ together with the simulation time t .

To do this a variable P is defined such that it is 1 when the system has reach ignition, $t = t_{\text{ig}}$, and zero when $t = 0$. An equation, which fulfill these requirements, is

$$P = \int_{t=0}^{t_{\text{ig}}} \frac{1}{\tau_{\text{ig}}(T_{\text{m}}(t))} dt. \quad (4.24)$$

The calculation process of this model could be easier to understand in terms of a stepwise explanation. Before the calculation starts one sets the parameters, T_{max} and r_{s0} , to what is desirable. Then a time step Δt is set and the calculations can start. For each time step, some heat diffuses away, and a new temperature, $T_{\text{m}}(t + \Delta t)$, is obtained from equation (4.19) or (4.23). Based on this new temperature a new ignition delay time, $\tau_{\text{ig}}(T_{\text{m}}(t + \Delta t))$, is obtained, which gives a new contribution to the variable P . If all the contributions add up to 1, the current parameters and conditions have produced an ignition. If not, P will stagnate and the process will count as a non ignition case.

As seen from Figure 4.2, the lower the temperature gets, the higher the ignition delay time gets, which means that the term $1/\tau_{\text{ig}}(T_{\text{m}}(t))$ in equation (4.24) gets smaller. If heat is diffused away too quickly P will never reach 1.

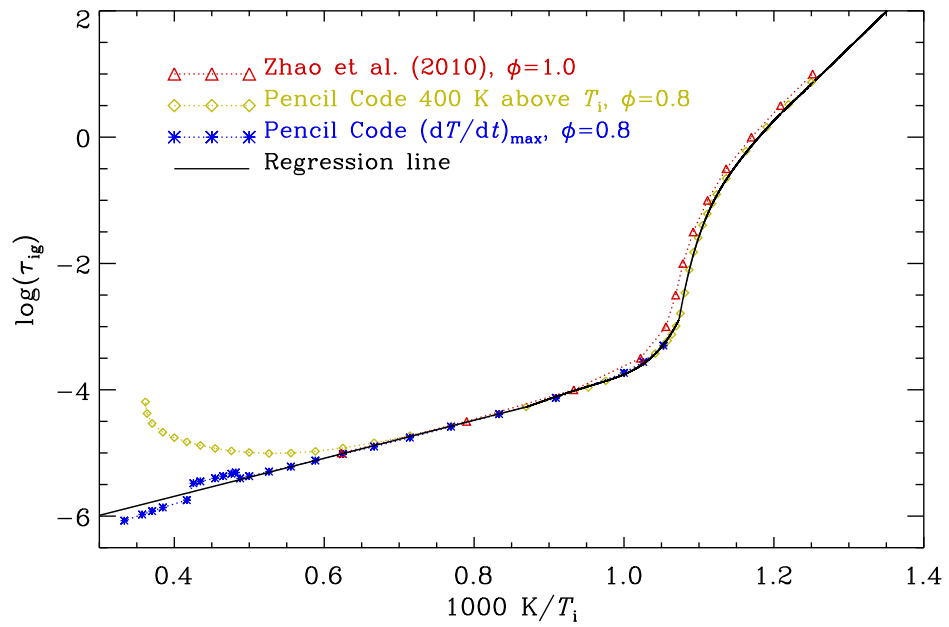


Figure 4.2: The graph shows the ignition delay time as a function of the initial temperature. The value of the axis are typically given as, $\log(\tau_{ig})$ and $1000 K/T_i$. The red data points are taken from Zhao et al. (2010) [9].

Chapter 5

Results

5.1 Ignition and the spatial design of the heat source

Ignition is affected by how heat is distributed inside a given domain. What the results in this section will show is how the width and the maximum temperature, r_{s_0} and T_{max} , affects ignition. This is done in the light of minimizing the ignition energy. The temperature distribution is chosen to be Gaussian as described in chapter 3. Furthermore, simulations from the simple model will be shown and compared with the Pencil Code method. The width of the temperature distribution which is considered for these simulations reaches from $r_{s_0} = 0.01$ cm to $r_{s_0} = 0.1$ cm.

5.1.1 The result from the Pencil Code

As mentioned in section 3.3.3, the simulation scheme is constructed such that the radicals in the mixture do not exist prior to the start of the simulation. In an experimental setting, with a spark ignition for instance, it would take an amount of time for the gas mixture to get heated to its final temperature. During this heating process the radical concentration in the mixture will increase near the source. When the heating source then is removed and there exists a temperature distribution in the system, the mixture will already contain an initial radical concentration. With this in mind one could state that the simulations in the Pencil Code have achieved a temperature profile infinitely fast. Experiments are typically performed with an induction time in the range of 5 ns to 1 ms [10], [11], [12]. The induction time is a measure of the time an external source is held in a combustion chamber before it is turned off. Considering that the simulations span about 0.3 ms and have a time step Δt of about 0.01 – 0.04 μs the results should be comparable with

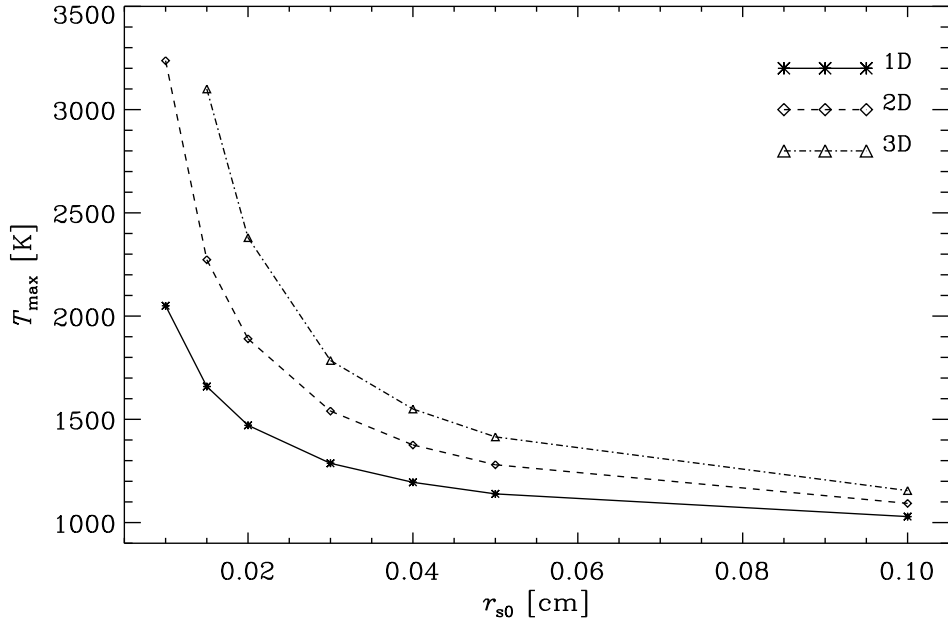


Figure 5.1: The results shown are from the Pencil Code and are done with the following parameters, $\phi = 0.8$, $T_0 = 300$ K and $P = 1$ atm. It shows how the Gaussian temperature distribution needs to be shaped in order for ignition to be reached. The number of grid points in the simulations are 128^N .

the studies of low induction time.

The results of the Pencil Code simulations are shown in Figure 5.1. It shows the necessary T_{max} to reach ignition for each r_{s0} . From the figure it can be seen that the necessary temperature needs to be increasingly higher as the width, r_{s0} , is decreased. This tendency can be seen in all the three simulations, but it gets stronger for higher dimensions. Also the temperature for the different dimensions seems to coincide as the radius gets larger. In general the temperature is higher as one moves up in dimensions.

For each of the radii, the domain of the system is adjusted to give a good resolution and the number of grid points for these simulations are set to be 128 in each dimension. When the number of grid points were increased to 256, the results stayed the same.

The simulation set done in 3D does not show any result for the case where $r_{s0} = 0.01$ cm. At this point no ignition was produced even at temperatures towards 5000 K.

5.1.2 The results from the simple model with different α 's

There are different set of results from the simple model regarding how the thermal diffusivity, α , is chosen. In Figure 5.2 the results are compared with each other together with the Pencil Code results. To get an easier overview of the comparison, only results from the 2D simulations are shown.

From Figure 5.2 it can be seen that the two cases, where α is constant, do not overlap the results of Pencil Code as good as the last Simple Model case, where α depends on temperature. This outcome was anticipated since the thermal diffusivity indeed does depend on temperature. However, for larger source radii the constant case where $\alpha = 5\text{cm}^2/\text{s}$ seems to coincide well. They overlap in the region where r_{s_0} is larger than about 0.03 cm and then separate. The main explanation for this, regarding better results with higher radii, lies in the fact that the larger the radius of the ignition source is, the less receptive the temperature of the ignition source is to diffusion. When it is less receptive, the initial temperature necessary for ignition can be lower, which means that the temperature from the initial state until ignition varies less. Therefore, when the temperature does not change considerably, the thermal diffusivity will stay more unchanged. It can also be seen that when $\alpha = 9\text{ cm}^2/\text{s}$, the results propose an overall higher temperature for large radii, but for small radii it still does not show the same rapid increase in T_{max} as the results do for the Pencil Code and the simple model with $\alpha = \alpha(T_m)$.

From Figure 4.1 it can be seen that a α value of $5\text{ cm}^2/\text{s}$ and $9\text{ cm}^2/\text{s}$ represents a temperature of about 1300 K and 1900 K respectively. By using a constant α , it would mean that the model uses an underestimated α when T_m is higher than the constant temperature value α corresponds to.

Therefore, it is chosen to mainly focus on the most accurate version of the simple model. Further details on the two different Simple Models can be seen in section 4.2.1 and 4.2.2.

5.1.3 Comparison of the simple model with $\alpha(T_m)$ and the Pencil Code

In Figure 5.3 the simple model results with $\alpha = \alpha(T_m(t))$ can be seen for all the dimensions. They are compared side by side with the results from the Pencil Code. The simple model with constant thermal diffusivity is not compared beyond the comparison in Figure 5.2 because of their lack in reproducing the Pencil Code results. From Figure 5.3, the simple model, which includes the thermal diffusivity's dependency on temperature, is very close to the Pencil Code results in all dimensions.

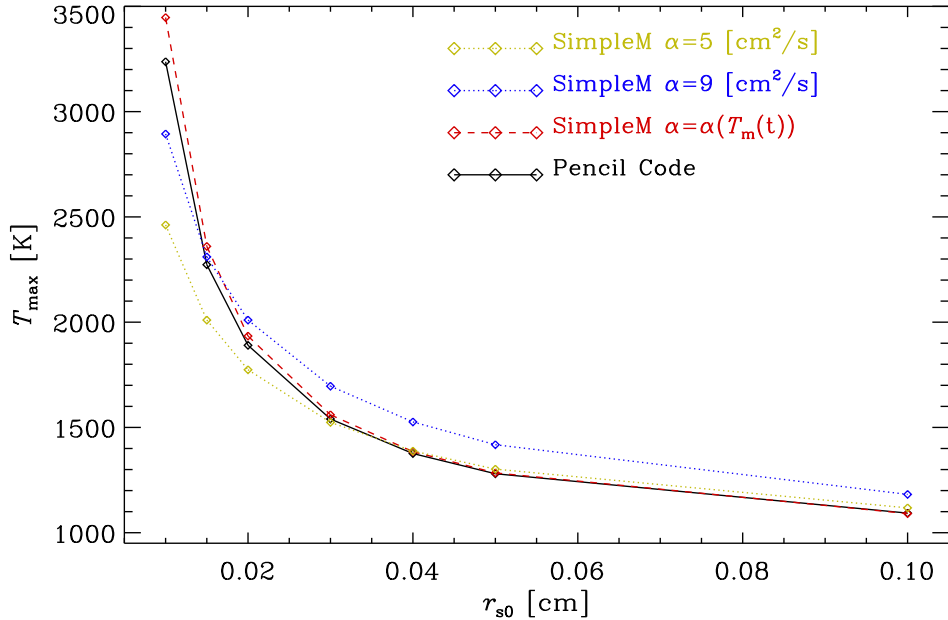


Figure 5.2: These results are from the simple model and compare the different α assumptions. To make the comparison easier, only the 2D results are shown. The Pencil Code result can also be seen in the figure.

It can be seen from the figure that the simple model have a small tendency to overshoot the Pencil Code results for 1D and 2D, but for the 3D case it seems that the opposite is true. However, in general the result is surprisingly good.

As mentioned, the Pencil Code lacks data for the 3D case where the radius is equal to 0.01 cm. This is found by the simple model to be 5640 K. This temperature is tremendously high and is an enormous increase from where $r_{s0} = 0.015$ cm. To be able to show the other results in Figure 5.3 properly, this point has not been included.

5.1. IGNITION AND THE SPATIAL DESIGN OF THE HEAT SOURCE

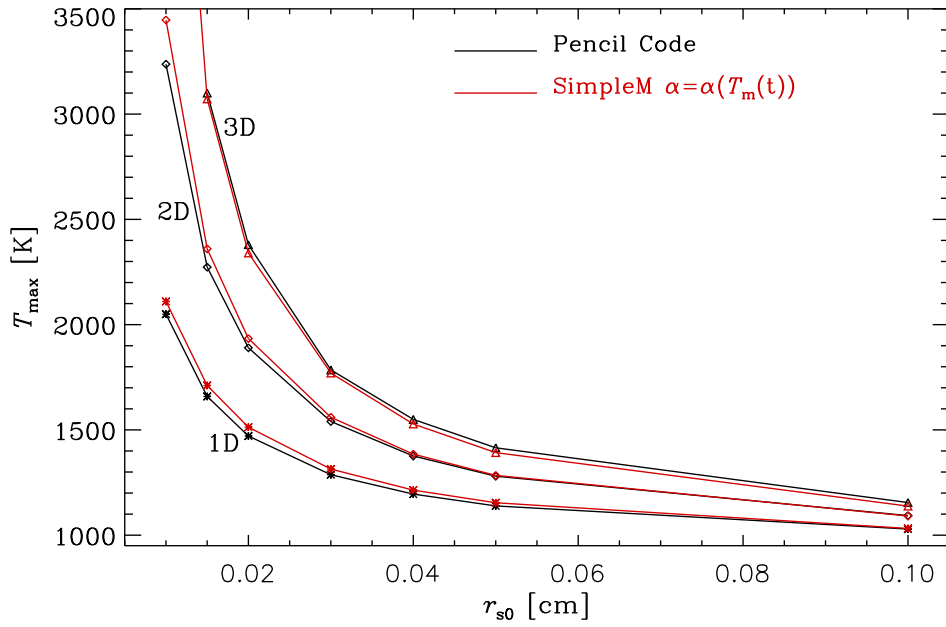


Figure 5.3: In this figure the results from Pencil Code and the results from the simple model are compared for all the dimensions. The parameters are $T_0 = 300$ K, $\phi = 0.8$ and $P = 1$ atm.

Table 5.1: MIE's dependency on the heat source radius

Geometry	$E(r_{s_0})$	Domain
1D	$422.4 r_{s_0}^{0.83}$	$r_{s_0} \in [0.01, 0.1]$ cm
2D	$713.2 r_{s_0}^{1.70}$	$r_{s_0} \in [0.01, 0.1]$ cm
3D	$1310.5 r_{s_0}^{2.62}$	$r_{s_0} \in [0.015, 0.1]$ cm

5.2 MIE of the heat source

This section presents the MIE results based on the simulations from the Pencil Code. The MIE is calculated according to section 3.4 and the results are shown in Figure 5.4. The figure also show the simulation results from Maas et al. (1988) [10] and Kim et al. (2004) [11], where the first one is based on a stoichiometric hydrogen-oxygen mixture, whereas the second one is based on a stoichiometric hydrogen-air mixture ($\phi = 1$). Both Maas and Kim have $P = 1$ atm and $\tau_s = 1 \mu s$, where τ_s is the energy duration time (induction time). The figure has logarithmic axis in order to see and compare the results in a proper way.

The figure denotes the proposed MIE from Glassman et al. [3] of 0.018 mJ. This result is based on experimental results from Calcote et al. [13] and Blanc et al. [14], and was found when $\phi = 0.8$.

For each of the Pencil Code simulations, a power regression analysis has been performed in order to see its dependency on the source radius, r_{s_0} , in the given domain. The dependency can be seen in Table 5.1 and Figure 5.4.

Figure 5.5 shows the energy densities of the different dimensions. The density is found by dividing the different energies by the unit length, the unit area or the unit volume, dependent if it is 1D, 2D or 3D. From the figure it can be seen that the energy density curves follow the same tendencies as in Figure 5.1.

5.2. MIE OF THE HEAT SOURCE

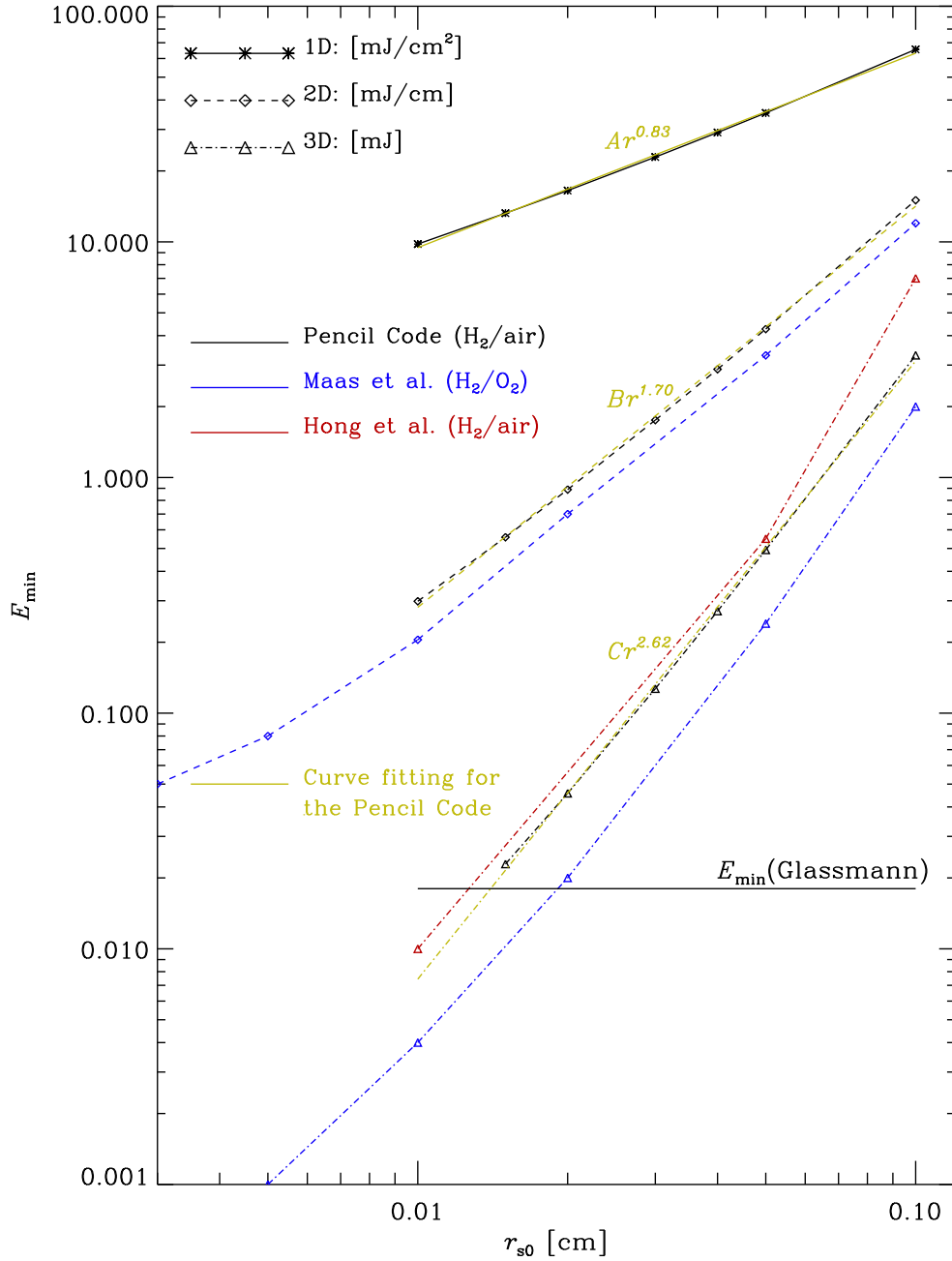


Figure 5.4: In this graph the MIE results from the Pencil Code can be seen in 1D, 2D, and 3D, and they are also compared with simulation results from Maas et al. (1988) [10] and Kim et al. (2004) [11]. For each of the result from the Pencil Code, a curve fitting line shows the MIE dependency on r_{s0} . Also the MIE proposed in Glassman et al. [3] based on experimental results are shown.

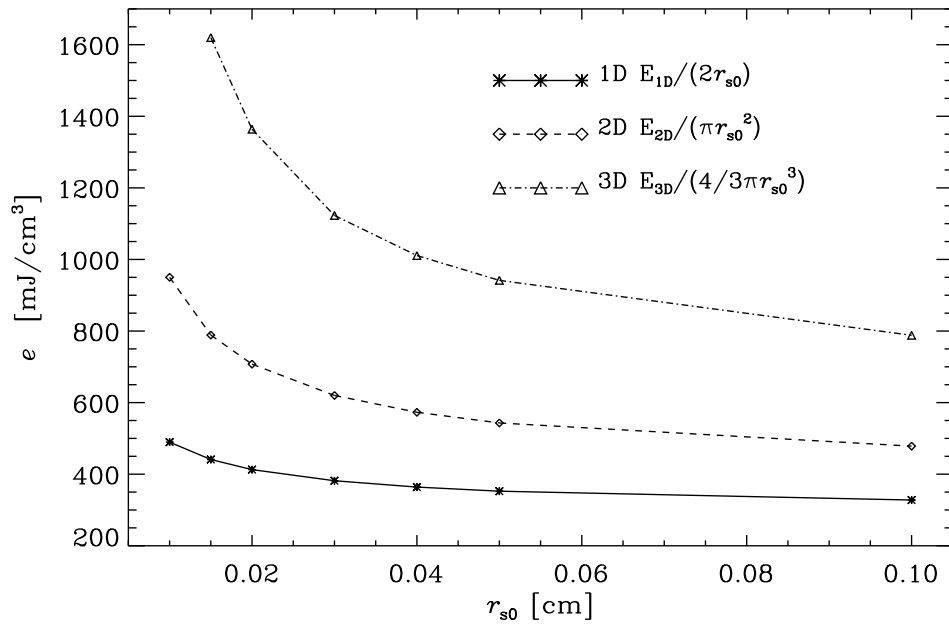


Figure 5.5: From this graph the MIE density from the Pencil Code results can be seen. The figure denotes how the densities are obtained.

Chapter 6

Discussion

6.1 Ignition and the spatial design of the heat source

6.1.1 The Pencil Code

In Figure 5.1 there are certain tendencies which can be noticed. It can be seen that the three simulation sets show the same tendency to have an increasing T_{\max} as the radius, r_{s_0} gets smaller. This behavior amplifies itself as the spacial dimension of the simulations are increased. These patterns can largely be explained by diffusion of heat.

For small radii, heat is diffused away from the center more quickly than for larger radii. This can intuitively be understood, because at the same amount of time, a wide distribution will be able to retain a higher portion of its initial temperature profile, than a narrow one. Then to achieve ignition for a very peaked distribution, a very high T_{\max} is needed since the radicals in the mixture need some time to build up their concentrations. If the temperature drops to quickly, below a certain value, the radical production will come to a stop and no ignition will occur.

One can also see this argument by looking at equation (4.18), which states that

$$\frac{\partial T_m(t)}{\partial t} \sim -\frac{(T_m(t) - T_0)^{\frac{2+N}{N}}}{r_{s_0}^2}. \quad (6.1)$$

This equation tells how the center temperature, $T_m(t)$, depends on the initial source radius. One can see if the radius is small, the temperature will drop quicker than if it is large. Even though equation (4.18) is derived for the simple model, and there are some simplifications related to it, it gives a good indication of why the results in Figure 5.1 look as they do.

The simulations from the Pencil Code in Figure 5.1 also show that the dimensionality has a large impact on the results. The 3D simulations, in general, need higher temperatures than the other two and so on. The reason that there is this difference has to do with what the radius of the heat source represents for the different dimensions, which then relates to how diffusion of heat operates. The radius of the heat source, r_{s_0} , for 1D, 2D and 3D represents respectively, the length on a line, the radius of a circle and the radius of a sphere.

For the 3D case, the temperature is Gaussian distributed in all the directions in the form of a sphere. In other words, if a spherical coordinate system is used to explain the distribution, θ and ϕ will be symmetric for any constant r . This source has the shape of a point in space and implies that heat will be diffused equally in all directions.

However, in the 2D simulations, the geometry of the distribution is reduced to a circular plate in a 2D-plane. For cylindrical coordinates this would represent a symmetric θ for any given r in the plane where $z = 0$, which would be the same as to use polar coordinates. Diffusion in this case would limit itself to apply only in the 2D-plane, which is natural because of the dimension in which the simulation is done. But if one imagines this two dimensional distribution in 3D, and for it to have no diffusion in the z -direction, the distribution would need to be an infinite long cylinder. Heat diffusion only occurs where there is a temperature difference, and since this cylinder would be symmetric about the plane where $z = 0$, no diffusion would happen along this direction.

Lastly, the 1D case is a temperature distribution along a line which is symmetric around the point where $r = 0$, see Figure 3.3.1. Here there is only diffusion of heat along this line, and from the center of the distribution there are then only diffusion in two directions. To try to see what spatial design this heat source would have in a 3-dimensional space, the 3D structure would need to represent a geometry where diffusion of heat only occurs in two directions. A geometry which could fulfill this requirement is an infinite plane in space.

The Laplace operator which is used in the heat equation differs from itself depending on dimension, coordinate system and symmetrical terms. For the three cases discussed above, the 1D, 2D and 3D case, the Laplace operator is given as equation (4.5), (4.6) and (4.7). This effects the heat equation, and as seen from equation (4.9), which was developed for the simple model, one sees that it effects how fast the center temperature drops. For the cases where heat diffusion causes the center temperature to drop quicker one would need a higher T_{\max} or a larger r_{s_0} to reach ignition.

The point to be made here is that it seems as diffusion of heat, which is much determined by the spatial design of the heat source, can explain the

6.1. IGNITION AND THE SPATIAL DESIGN OF THE HEAT SOURCE

ignition results in Figure 5.1.

As the radius get sufficiently large the results for all dimensions seem to coincide, as diffusion of heat gets less important. According to the explosion limits, (Figure 2.1), the lowest temperature for ignition with 1 atm is about 850 K. This appears to be in good accordance to the temperature the results in Figure 5.1 seems to coincide towards.

6.1.2 The simple model

The results from the simple model are plotted alongside with the results from the Pencil Code in Figure 5.3. The goal of the simple model was to try to reproduce the results from the Pencil Code. As seen from the results, the simple model is capable of reproducing results from the Pencil Code despite its simplifications.

In general the results overlap best for large radii and tend to deviate more for the smaller radii. This effect show itself in the 1D case and especially in the 2D case which has the largest deviation of about 200 K for the smallest radius of 0.01 cm. For the 3D case it would then be natural to anticipate an even larger deviation for small radii, but as seen in the figure this is not the case. In 3D, the simple model curve follows the curve of the Pencil Code good for all radii, but in contrast to the 1D and 2D results, the simple model curve tends to lie somewhat beneath the Pencil Code curve.

6.1.2.1 Simplifications

The simplifications done in the Pencil Code method compared to a real life ignition event also apply for the simple model. In addition the simple model only solves the heat equation and do not include chemical reactions. This means that there is not generated heat in the simulations and the temperature, T_m , will only drop according to the heat equation as time goes by. The Pencil Code on the other hand, models all the chemical equations alongside with the heat equation. Because of this, it is natural to believe that the center temperature, T_m , will decrease quicker with the use of the simple model, than with the use of the Pencil Code. A faster temperature decrease implies that a higher T_{\max} would be needed for ignition. For the particular case used in Figure 6.1 it can be seen that T_{\max} is higher in the simple model. This figure shows the time development of the center temperature, T_m , for both methods and is taken from the 1D results in Figure 5.3 where $r_{s_0} = 0.03$ cm. As seen, T_m decreases more for the simple model than for the Pencil Code. This deviation is small in the beginning, but increases as there is produced more and more heat in the Pencil Code case. The vertical blue line in the figure indicates the time where the variable P , equation (4.24) in the simple

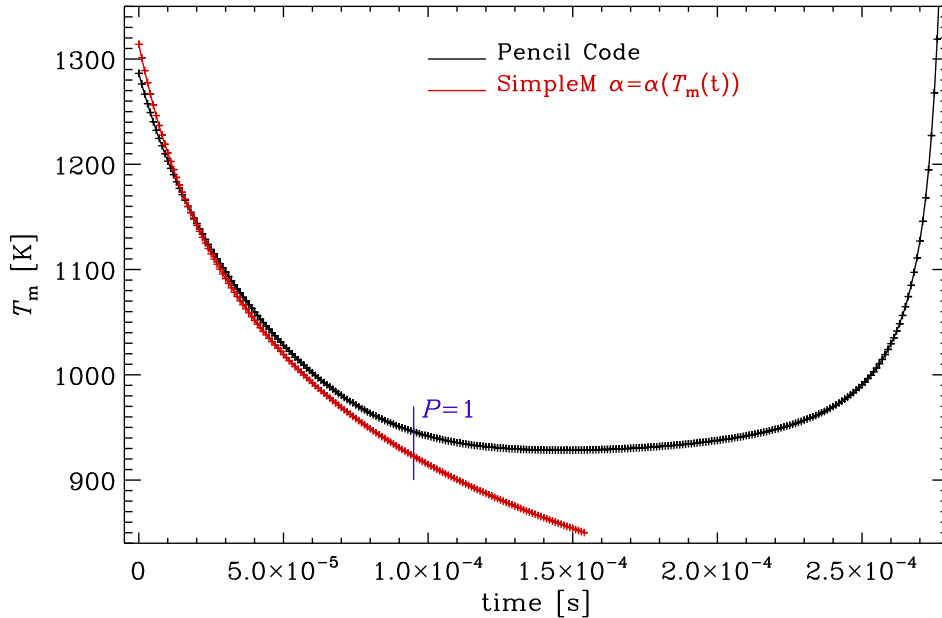


Figure 6.1: This figure shows how the temperature evolves with time. The red line is from the simple model and the black line indicates the result from the Pencil Code. The vertical line denotes at what time the variable P has reach one. Both simulation are done in 1D with $r_{s_0} = 0.03$ cm. The initial center temperature, T_{\max} , needed for ignition is equal to 1314 K for the simple model and 1287 K for the Pencil Code.

model, has reach one. One can notice that the differences in temperature do not show itself in any large parts before after the time is such that $P = 1$. By looking at both Figure 4.2 and equation (4.24) it can be noticed that a higher temperature contributes more on the variable P 's way towards one than a lower temperature. The fact that the highest temperatures in the simple model simulations are present where the time is small, indicates that the most essential part for ignition determination is in the beginning of the simulations. Since it is here that the simple model overlap best with the Pencil Code, the simple model models close to the true temperature, which affects in using the right data from the ignition delay time results (Figure 4.2). What this signalizes is that the temperature in the ignition simulations follow close up to what the heat equation suggests alone, and is a major reason for the accuracy of the simple model.

However, the small deviations in how fast T_m drops, could explain the results for the 1D and 2D simulations, in that the simple model needs somewhat higher temperatures for ignition.

Another simplification which is done in the simple model has to do with the temperature distribution. As stated before, the simulation performed in the simple model only models the center temperature of the distribution. The equation for the center temperature is obtained from the Gaussian distribution together with the heat equation, as described in section 4.2.2. Furthermore, a relation between the height and the radius of the Gaussian temperature distribution, $T_m(t)$ and r_{s0} in equation (4.17), was established by the assumption that the area under the curve was constant. This relation was needed in order to solve equation (4.9). But basically the quantity which is really constant is the thermal energy of the temperature distribution. If one had incorporated the conservation of energy in the simple model, the specific heat and the density would have had to been included as functions of temperature in equation (4.10), (4.11) and (4.12). Since they are not, the relation between the height and the radius of the distribution will cause some inaccuracy between the simple model and Pencil Code.

6.1.2.2 Advantages and disadvantages

The advantages of the simple model are its simplicity alongside with its ability to reproduce the numerical calculations from the Pencil Code. For this particular task, to find the temperature distribution which gives ignition, it has proven itself powerful. The calculation power needed in the simple model to obtain the results can easily be done on a personal computer and are less time consuming than a method where all the physical equations of the problem are solved on a large grid. This is especially true when simulations in three dimensions are handled. Considering the results the simple model has produced for the hydrogen-air system, there seems to be no reason why it should not be able to predict the same accurate result for a more complex mixture. If this is the case, it would be a very useful way of determining the geometry of the necessary ignition source.

The disadvantage is that one needs external information about the thermal diffusivity, $\alpha(T)$, and the ignition delay time, $\tau_{ig}(T)$, for the particular combustible mixture. In addition, a curve fitting analysis must be performed to transform the data into a function which can be read by the model. Furthermore, the model can only predict what it has been designed to predict and does not give any other outputs.

6.2 MIE

The following section will mainly treat the results in Figure 5.4. This figure shows the energy of the simulations in Figure 5.1, instead of T_{max} . The energy is calculated based on the initial temperature distribution, and since T_{max} is

minimized, for the given r_{s_0} , the energy obtained will be the MIE. From the figure one can see the three simulation sets in 1D, 2D and 3D obtained from the Pencil Code in a log-log plot. How the energies in the different dimensions are defined are shown in the upper left corner of Figure 5.4.

The three data sets show a large difference in energy; about an order of magnitude. This has to do with what the energy represent for the different dimensions. In the 1D case, the energy is given as $[\text{mJ}/\text{cm}^2]$ and actually represent the energy necessary to heat up a plane of 1 cm^2 with the width of $2r_{s_0}$. The width, in the sense that r_{s_0} is not a definite width, but a type of standard deviation in a Gaussian distribution. The same goes for the 2D results, which is given as $[\text{mJ}/\text{cm}]$ and represents a cylinder with radius r_{s_0} and the length of 1 cm . This means that the 1D and 2D cases are given as two different types of energy densities. The 3D simulations on the other hand represent the actual energy since it is given as $[\text{mJ}]$ and is the energy necessary to heat a sphere with a radius of r_{s_0} .

From the figure it can be seen that the results in the different dimensions have different slopes. In advance, one could have approximately anticipated the energy dependency on r_{s_0} as linear, quadratically and cubically, since the volume goes as r^3 , the area as r^2 , and the length as just r . As r_{s_0} changes in the different cases, it would represent a change in the length, area or volume for the different dimensions, which means that if the center temperature where constant for the different radii, it would probably have been the case. However, since the center temperature increases for lower radii, as shown in Figure 5.1, it is believable that the energy dependencies will lie somewhat lower than first indicated.

A power regression analysis of the energies as functions of r_{s_0} can be seen in Figure 5.4 and Table 5.1. In great deal, the analysis confirms the suspicion above. Furthermore, the energy dependency on the radius in 3D, which is $r_{s_0}^{2.62}$, deviates more from a cubically dependency, than the other two deviates from a quadratically and linear dependency. This relates to the fact that the results in 3D demands higher increase in temperatures for low radii, than what is the case for the 1D and 2D results. An other way to look at it, is by equation (2.22), which shows the energy necessary to heat a sphere uniformly to a desired temperature. From this equation it can be seen how the energy depends on the temperature and the radius, and since it is shown in Figure 5.1 that the temperature is close to inversely proportional to the radius, it is natural to believe that the overall dependency on the radius will lie lower than a cubically one.

In Figure 5.5 the energy densities can be seen for each dimensionality. They have been calculated to compare the different energies in the same reference system, i.e. with the same energy unit, $[\text{mJ}/\text{cm}^3]$. The energy density values themselves do not provide much useful information, but when

seen together they show certain trends. Since the radius dependency is taken out of the equation, the energy densities amplify the other variables that the energy depends on, such as specific heat, density and temperature. If one compares Figure 5.5 and Figure 5.1, it can be seen that they share much of the same characteristics. This leads to the conclusion that, except from the radius of the temperature distribution, it is the dependency on the temperature which has largest influence on the energy.

As mentioned, the 3D simulation with $r_{s_0} = 0.01$ cm did not produce any ignition and it could be speculated in that the reason is related to condition (2.25) in section 2.5, which states that $r_f \gtrsim 3.7a$, where $a = \alpha/S_L$ is the thermal width of the flame. This condition were obtained for a sphere with radius r_f , and if it is met, the layers just outside the initially ignited mixture will have time to further ignite before the volume cools. If one inserts the values from our system, one could get an indication of how small this condition allows the radius to be. The value for the thermal diffusivity is gained from Figure 4.1 and the laminar flame speed is obtained from a paper by Dong et al. (2009) [15]. Dong et al. proposes that $S_L \simeq 170$ cm/s in a H_2 /air mixture. The value $\alpha \simeq 0.5$ cm²/s is taken from Figure 4.1 at a temperature equal to 300 K, since this is the ambient temperature. The result then becomes $r_f \gtrsim 0.011$ cm. Straight forward this condition suggests that no ignition should be expected where the sphere radius is equal to 0.01 cm. However, it is more complicated since the heat source used here is Gaussian distributed, and not an uniformly heated sphere with a well defined transition. For a Gaussian distributed profile it would perhaps be more correct to use a value for the thermal diffusivity which reflects a higher temperature, since the outside layers of the temperature core would already be heated additionally with respect to the ambient temperature. In that case, the condition would impose a larger limit regarding the radius of the sphere.

Another plausible explanation could be that the reaction mechanism used is not designed for such high temperatures which $r_{s_0} = 0.01$ cm would imply. According to the simple model a $T_{\max} = 5640$ K would be needed.

In Glassman et al. [3] the minimum ignition energy is stated to be equal to 0.018 mJ for hydrogen. If one assumes that the curve fitting function in 3D for the Pencil Code results continue downwards, the MIE by Glassman et al. would propose a r_{s_0} of about 0.014 cm.

In experiments regarding the ignition energy, they are often conducted by the use of an electrical spark to ignite the gas. The paper by Ono et al. (2006) [12] showed the MIE to be equal to 0.017 mJ, which is close to the one proposed by Glassman et al. It was shown that in order to produce this MIE result, the gap distance was needed to be set equal to 0.5 mm. The geometry of an electrical spark could be looked upon as a cylinder in space and if one draws a parallel to this study, the results, in which would be

equivalent to that geometry, is the 2D simulations. The gap distance would be the length of the cylinder, thus would it be the height of the 2D cross section. If one assumes that the radius of the spark is about 0.01 cm one could take the result from the 2D simulation with $r_{s_0} = 0.01$ cm, which is about 0.3 mJ/cm, and multiply it with the gap distance of 0.05 cm. One would then obtain the MIE for this imitated spark, which would be equal to 0.015 mJ. But sure enough, this result lies under the assumption that one looks away from the endpoint of the cylinder. Since there would be heat diffusion at the endpoints, it would be expected that the MIE would lie a bit higher.

The two results from Maas et al. can also be seen in the figure. One of them has cylindrical geometry and the second one has a spherical geometry. These numerical results are done for a stoichiometric hydrogen-oxygen mixture and are compared with the Pencil Code results. The fact that the Maas et al. simulations have lower energies could be explained in that it is a hydrogen mixture in pure oxygen while the simulations in Pencil Code are for a hydrogen-air mixture. The Maas et al. results also show energy values for radii down towards $r_{s_0} = 0.003$ cm. For these low radii, the 3D simulation suggests a MIE which is much lower than the experimental results.

From the study by Kim et al. it is suggested a MIE of about 0.01 mJ for $r_{s_0} = 0.01$ cm. This value also seems to contradict the experimental MIE values from Glassman et al. [3] and Ryo Ono et al. [12]. The fact that the Pencil Code corresponds well with the experimental data, regarding the MIE, is a good indication of the method's credibility.

Chapter 7

Conclusion

In this thesis it has been shown by DNS with the Pencil Code that the geometry and shape of the heat source have a strong effect on ignition. The heat source was modeled by a Gaussian temperature distribution and the effect was seen when the dimensionality and size of the distribution was altered. The 3D simulations with spherical geometry required higher temperatures than the 2D simulations with cylindrical geometry. In addition, the narrower the temperature distributions were, the higher the temperatures needed to ignite the gaseous mixture became. This was mainly related to the magnitude of which heat diffused away with the varying geometries.

A new ignition model, "the simple model", was proposed with the goal of simplifying the physical elements included in the simulation while still producing accurate results. The element on which the model was based was the heat equation with input data from ignition delay time simulations. It has been validated through simulations that the simple model accurately replicated the results from the Pencil Code for the studied hydrogen-air mixture.

Regarding the MIE results, it was clear that it mainly depended on the radius of the Gaussian temperature distribution. The MIE was lowest for the lowest radii which gave ignition. Furthermore, it seemed to be a lower limit of how small the radius could be for the different geometries. In 3D, this limit reflected a MIE which agreed well with the experimental results.

Bibliography

- [1] The Pencil Code
<http://code.google.com/p/pencil-code/downloads/list>
- [2] K. J. Laidler, "CHEMICAL KINETICS" Third edition (1987)
- [3] I. Glassman and R. A. Yetter "Combustion" 4th Ed., (2008)
- [4] Chemical-Kinetic Mechanisms for Combustion Applications, University of California, San Diego
<http://maeweb.ucsd.edu/~combustion/cermech/index.html>
- [5] J. Li, Z. Zhao, A. Kazakov and F. Dryer, "An updated comprehensive kinetic model of hydrogen combustion", Int J Chem Kinet 36 (2004), pp. 566-575.
- [6] T. Turanyi at the Institute of Chemistry ELTE, Budapest "Chain reactions" PowerPoint presentation
garfield.chem.elte.hu/Turanyi/Chain_reactions.ppt
- [7] The Pencil Code Manual
<http://www.nordita.org/software/pencil-code/doc/manual.pdf>
- [8] N. Babkovskaia, N. E. L. Haugen, A. Brandenburg, "A high-order public domain code for direct numerical simulations of turbulent combustion" (2010)
- [9] Z. Zhao, Z. Chen & S. Chen "Correlations for the ignition delay times of hydrogen/air mixtures" (2010)
- [10] U. Maas and J. Warnatz, "Ignition Processes in Hydrogen-Oxygen Mixtures" COMBUSTION AND FLAME 74: 53-69 (1988)
- [11] H. J. Kim, S. H. Chung and C. H. Sohn, "Numerical Calculation of Minimum Ignition Energy for Hydrogen and Methane Fuels" KSME International Journal, Vol 18 No. 5, pp.838-846, (2004)

BIBLIOGRAPHY

- [12] R. Ono, M. Nifuko, S. Fujiwara, S. Horiguchi and T. Oda, "Minimum ignition energy of hydrogen-air mixture: Effects of humidity and spark duration", *Journal of Electrostatics* 65 (2007) 87-93
- [13] H. F. Calcote, *Ind. Eng. Chem.* 44, 2656 (1952)
- [14] M. V. Blanc, *Proceedings of the Combustion Institute* 3, 363 (1949)
- [15] C. Dong, Q. Zhou, Q. Zhao, Y. Zhang, T. Xu, S. Hui "Experimental study on the laminar flame speed of hydrogen/carbon monoxide/air mixtures" (2009)